The Autism Risk Factor CHD8 Is a Chromatin Activator and Functionally Dependent on the ERK-MAPK Pathway Effector ELK1

Bahareh Haddad Derafshi[1], Tamas Danko[1,3], Soham Chanda [1,2,], Pedro Batista[5,8] , Ulrike Litzenburger[5,9], Qian Yi Lee[1,3], Yi Han Ng[1,2] , Anu Sebin[1,3], Howard Y. Chang [4,5,6,7], Thomas C. Südhof [2,4], Marius Wernig* [1 ,3]

[1]Institute for Stem Cell Biology and Regenerative Medicine, [2]Department of Molecular and Cellular Physiology, [3]Department of Pathology, [4]Howard Hughes Medical Institute, [5] Center for Personal Dynamic Regulomes, [6]Program in Epithelial Biology[7,] Department of Genetics,
265 Campus Drive, Stanford, CA, 94305, USA
[8]Current address: Laboratory of Cell Biology, Center for Cancer Research, National Cancer Institute, National Institutes of Health, Bethesda, MD 20892, USA
[9]Current address: Celgene, San Francisco, CA, 94158, USA.

* Correspondence: wernig@stanford.edu

Abstract

The chromodomain helicase DNA-binding protein CHD8 is among the most frequently found de-novo mutations in autism (1-3). Unlike most other autism-risk genes, *CHD8* mutations appear to be fully penetrant (4). Despite its prominent disease involvement, little known about its molecular function. Based on sequence homology, CHD8 is believed to be a chromatin regulator, but mechanisms for its genomic targeting and its role on chromatin are unclear. Here, we developed a human cell model carrying conditional *CHD8* loss-of-function alleles. Full knockout CHD8 was required for the viability of undifferentiated human embryonic stem (ES) cells, whereas postmitotic neurons survived following CHD8 depletion. However, chromatin accessibility maps and transcriptional profiling revealed that CHD8 is a potent general chromatin activator, enhancing transcription of its direct target genes, including a large group of autism genes. CHD8's genomic binding sites in human neurons were significantly enriched for ELK1 (ETS) motifs. Moreover, positive CHD8-dependent chromatin remodeling was enhanced at ELK1 motif-containing CHD8 binding sites. ELK1 was the most prominent ETS factor expressed in human neurons and was necessary for CHD8 to target the sites that contained the ELK1 motif, demonstrating a cooperative interaction between ELK1 and CHD8 on chromatin. We also observed potential role of CHD8 in ELK1 localization on nuclear compartments in a transcription-stage-dependent manner. Finally, inhibition of ELK1 activity or ELK1 knockdown that enhances the neurogenesis from embryonic stem cells (ES) was dependent on the presence of CHD8. In summary, our results establish that CHD8 is a strong activator of chromatin accessibility and transcription in neurons and reveals a role in regulating many high-risk autism genes. Additionally, we show there is molecular and

functional interdependence of CHD8 and ELK1 in chromatin binding of CHD8, nuclear interaction of ELK1, and neurogenesis enhancement. These data imply the involvement of the MAPK/ERK pathway effector ELK1 in pathogenesis of autism caused by *CHD8* mutations (5).

To study the role of CHD8 in human neurons, we generated conditional loss-of-function alleles of *CHD8* in pluripotent stem cells and heterozygous and homozygous conditional knockout (cKO) cells. The heterozygous cKO allele was constructed by surrounding exon 4 with two loxP sites (Fig. 1a, Extended Data Fig. 1). Deletion of exon 4 is predicted to produce a frameshift and early termination mutation. We obtained two correctly targeted ES, and one correctly targeted iPS cell line (Extended Data Fig. 1a-c). To generate a homozygous cKO of *CHD8*, we applied the CRISPR/Cas9 system to induce an indel mutation in the non-targeted wild-type allele of the gene (Fig. 1b). This effort resulted in two homozygous cKO ES and one iPS cell lines (Extended Data Fig. 2b,e). To validate the conditional depletion of the CHD8 protein in targeted lines we used immunofluorescence and western blotting and we infected heterozygous and homozygous cells with Cre recombinase or ΔCre, a functionally inactive form of Cre and measured either the total levels of protein in neurons or the loss at individual cell by immunofluorescence assay in ES cells (Fig. 1d, Extended Data Fig. 2c). Indeed, CHD8 protein was fully depleted in homozygous cKO ES and neurons three days after infection with Cre, but not ΔCre (Fig. 1d, Extended Data Fig. 2c). Surprisingly, complete loss of CHD8 in human ES and iPS cells led to pronounced cell death within 5-7 days, but neurons survived the full depletion (Extended Data Fig. 2d).

We next characterized *CHD8*-mutant neurons and differentiated our targeted lines using a previously established protocol (6). In contrast to the pluripotent state, the depletion of CHD8 in differentiated neurons did not affect cell viability (Extended Data Fig. 2d). We used electrophysiology to reveal potential functional phenotypes. Intrinsic membrane properties of resting neurons were unchanged in CHD8-mutant cells (Extended Data Fig. 3a, e). Active membrane properties induced by stepwise current injection were similar between mutant and WT cells (Extended Data Fig. 3b, f). We found that the properties of synaptic transmission, such as evoked excitatory postsynaptic currents (EPSCs) were unchanged in heterozygous and homozygous mutant cells (Extended Data Fig. 3c, g). The frequency and amplitude of spontaneous miniature EPSCs in CHD8 heterozygous cKO cells were not statistically different from WT neurons (Extended Data Fig. 3d). Thus, loss of CHD8 did not grossly affect the intrinsic physiological and basic functional synaptic properties of human neurons using standard electrophysiology.

CHD8 is related to SNF2 helicase and ATP-dependent chromatin remodelers that generally affect transcriptional regulation (7-10). Since CHD8 is mutated in autism, we next wanted to

characterize its presumed function as chromatin remodeler in human neurons (11). To map its genomic binding pattern in human neurons, we generated a human ES cell line in which endogenous CHD8 is expressed with a C-terminal FLAG-HA-tag (Fig. 2a, Extended Data Fig. 4). Western blotting showed that tagged protein had the expected size (Fig. 2b). Then we performed ChIP-seq using antibodies against the HA tag and the N-terminus of CHD8 protein upon differentiation into neurons (Fig. 2g). ChIP-seq results from both experiments correlated well (Pearson r =0.87) (Extended Data Fig. 5d). In particular, strong CHD8 binding sites were enriched around transcription start sites (TSS) and not much enriched at distal enhancers (Fig. 2d, Extended Data Fig. 5e) (12). Notably, CHD8 binding correlated with active histone marks, particularly at promoters of actively transcribed genes with GO term related to chromatin regulation and transcription (Fig. 2e, Extended Data Fig. 5b, Extended Data Fig. 7g) (13).

Enrichment analysis showed that most CHD8 target sites contained YY1 and ETS motifs, and the odds ratio of ETS motif (Extended Data Fig. 6a) enrichment was higher in the strong binding sites compared to weaker binding sites (Fig. 2g, f, Extended Data Fig. 5c, f) (14). The ETS motif enrichment could not be simply explained by a bias towards the promoter regions as non-CHD8 occupied promoters lacked such enrichment (Fig. 2g). Accordingly, no ETS motif was found among the top 30 motifs enriched at CHD8 unbound promoters (Extended Data Fig. 6b, c). The average ChIP-seq signal intensity at promoters of downregulated genes was higher than at promoters of upregulated genes, suggesting that CHD8 acts primarily as a transcriptional activator at its target sites (Extended Data Fig. 7a). This conclusion was corroborated by a shift in the cumulative distribution of gene expression changes of CHD8-bound genes compared to unbound genes (Fig. 2h).

Quantification of gene expression by RNA-sequencing showed that heterozygous CHD8 mutant cells exhibited only subtle changes, as described before (15, 16). Nevertheless, results revealed upregulation in expression of a distinct group of activity-depend genes that previously described as an important gene module associated with ASD (Fig. 1e-left) (17). Gene expression changes were more pronounced in homozygous *CHD8*-mutant neurons and more genes are down than upregulated, consistent with overlapping genes between the two experiments, which were predominantly downregulated (Fig. 1e-right, 1f). In addition to synaptic and cell-adhesion molecules, we found several chromatin-related genes to be downregulated in *CHD8*-KO cells (Fig. 1e-right, Extended Data Fig. 7e, f). Many of the chromatin factors themselves are listed as ASD genes according to the updated SFARI gene list, suggesting CHD8 directly regulates these genes and their secondary downstream targets in neurons (18). Results showed there are more shared genes

between the overlapping downregulated, compare to upregulated genes between the two knockout experiments (Fig. 1f). Additionally, downregulated genes in CHD8 heterozygous and homozygous KO neurons had a higher association with CHD8 binding (Extended Data Fig. 7a). Similarly, results showed there are more shared genes between the overlapping downregulated, compare to upregulated genes between the two knockout experiments (Fig. 1f). ASD genes, in particular, were more enriched in downregulated group of genes (Fig. 1g). Collectively results suggest that functional bindings of CHD8 in neurons are mostly activating.

Disease Ontology (DO) and Gene Set Enrichment Analysis (GSEA) demonstrated that autism spectrum disorder and intellectual disability are associated with differentially expressed gene (DEG) list in neurons (Fig. 1h, Extended Data Fig. 7d). Gene ontology (GO) analysis result in pathways related to neurological disorders in heterozygous KO experiment; an encouraging finding that reveals even small changes in CHD8 level causes changes in gene expression that is biased to neurological disease pathways. Enriched GO terms from DEGs in homozygous KO neurons were generally related to two groups: “Synapse” and “Chromatin regulation” (Extended Data Fig. 7f). These two modules are an important group of genes that play a role in molecular pathology of ASD. The enrichment suggests that molecular pathways of ASD might converge on CHD8 targets (Extended Data Fig. 7f) (19, 20). When we investigated the ASD genes with CHD8 peak at promoters and also with significant gene expression change in KO, we observed >80% of the genes are downregulated, supporting our previous findings that CHD8 is an activator of its major molecular the disease-related targets (Fig. 2i).

Next, we performed ATAC-seq to assess the chromatin state of CHD8-mutant neurons (21, 22). Differential accessibility analysis revealed the vast majority of CHD8 mutant changes represent loss of accessibility; 1481 peaks lost accessibility compared to 106 peaks that gain accessibility in KO neurons (Extended Data Fig. 8b, e). Cross-correlation analysis of ATAC-seq signal and mapping reads for nucleosome positioning showed an increased nucleosome density at closed sites (Fig. 5d) (22). These results demonstrate that CHD8 mainly contributes to maintaining open and accessible chromatin. This finding is in accordance with transcriptional changes that we observed for all DEGs from CHD8 homozygous KO and for a subset of those genes with CHD8 binding on promoters; all were downregulated (Fig. 1e-left, Fig. 2h). Overall across the genome CHD8 binding enriched on sites with differential accessibility in KO cells, suggesting CHD8 regulates its chromatin mostly through direct genomic interaction (Fig. 3g). Closer inspection of the promoters of genes with change in RNA expression and statistically significant change in the ATAC-seq (n=136) revealed CHD8 binding strengthen at promoters of downregulated genes and on sites that loose accessibility in KO

neurons (Fig 3a). Similarly, a genome-wide analysis of “all” sites with differential accessibility in CHD8-KO revealed strong genomic interaction of CHD8 on closing sites compared to opening sites (Extended Data Fig. 8d, e).
Analogously, promoters that lost accessibility in ATAC-seq experiment also show a decrease in gene expression in CHD8 homozygous KO neurons (Extended Data Fig. 8c). Collectively, these observations demonstrate clearly that high-affinity binding sites of CHD8 in neurons are largely activating (Extended Data Fig. 5c, Extended Data Fig. 8e). Nevertheless, since CHD8 binding is enriched in ELK1 motifs, it`s chromatin activating role, in turn, is more pronounced on ELK1 motif sites (Fig. 3c). In accordance, motif enrichment analysis on ATAC-seq peaks and calculating odds ratio showed the ELK1 motif is enriched on sites with decreased accessibility (Fig. 4b, Extended Data Fig. 6a). Another important observation showed promoters of many chromatin modifiers regulated by CHD8, and the GO terms of genes, with differential accessibility in KO, is related to chromatin regulation (e.g., GO: 0005654; regulation of transcription) (Extended Data Fig. 7g).

Our findings show ASD genes that are among the targets of CHD8 in ATAC-seq, RNA-seq, and ChIP-seq experiment lost gene expression in KO (Extended Data Fig. 9a). Similarly, synaptic, neuronal activity-regulated genes, and prominent chromatin remodeling factors lost promoter accessibility in ATAC-seq and gene expression in RNA-seq experiment (Extended Data Fig. 10b,c). These results demonstrate that CHD8 is an activating chromatin factor on its genomic targets and disease-related targets. Additionally, we found CHD8 binds to promoters of a group of highly heritable mutant ASD genes, generally carrying biallelic recessive disruptive mutation. Members of ETS transcription factors with a role in serotonin neuron development are among this group of ASD genes; suggesting enrichment of ELK1 motif on targets of CHD8 might be related to the molecular pathology of ASD (Extended Data Fig. 9c) (23).

Next, we applied a multivariate hidden Markov model (HMM) to annotate genome-wide CHD8 targets using publicly available datasets for chromatin modifications from human H9-derived neurons and ChromHMM software (24, 25). An unsupervised modeling of epigenome revealed chromatin remodeling activity of CHD8 occurs non-preferentially at promoter and proximal enhancers, regardless of the activity of the genomic site, but direct bindings of CHD8 mostly seen on actively transcribed promoters (Fig. 4e).

To understand regulatory role of CHD8 and ELK1 motif in RNA expression, we divided CHD8 binding regions into upstream of ELK1 motif and downstream of ELK1 motif on either site of the transcription start sites (TSS). Then we proceeded with the pairwise-correlation analysis of RNA

expression (mean FPKM from wild type cells) with average CHD8 binding signal. We also divided the genome into three regions; based on the proximity to TSS, for the correlation analysis. Results demonstrate CHD8 binding upstream ELK1 motif sites at proximal promoters (-500) positively correlates with gene expression level, which suggests CHD8 binding upstream of ELK1 motif and transcription start sites potentially plays a role in regulating gene expression and chromatin accessibility (Fig. 3d-f). Similarly, gnome-wide, normalized, and binned (100 bp) CHD8 binding signal at the ELK1 motif sites showed an increase in CHD8 binding at upstream of ELK1 motif compared to downstream sites (Extended Data Fig. 7a).

Implementing cross-correlation to ATAC-seq signal and analysis of nucleosome positioning revealed marked increase in nucleosome occupancy at promotes with ELK1 motif. The change exclusively is at the position of nucleosome +1 of NFR sites, which shows the directionality of nucleosome remodeling in KO. The loss of accessibility in KO-ATAC-seq that arises from nucleosome repositioning is related to the canonical role of CHD8 as an ATP-dependent SNF2 nucleosome-remodeling factor that alters DNA and histone contacts and local chromatin structure (Fig. 5d, Extended Data Fig. 8f). We then investigated nucleosome remodeling across the genome (not only at the promoters), with centering the signals at the ELK1 motifs, we observed nucleosome occupancy shows no change. Moving away from the ELK1 towards the downstream of the motif direction (at ~ + 2Kb of motif), there is a significant increase in nucleosome signal in KO cells (Fig. 3b). Therefore, we concluded CHD8 regulates chromatin accessibility at downstream of the nearest ELK motif, suggesting directional and distributive chromatin remodeling activity.

Previous findings show *ELK1* is a downstream transcription effector of MAPK/ERK signaling pathway with suggested roles in the regulation of cellular homeostasis, such as apoptosis(26, 27). *ELK1* functionally interacts with the transcriptional machinery components and has a role in gene regulation (28-30). The similarity of *CHD8* and *ELK1* in the regulation of gene expression, alongside our findings that showed distinct role of *CHD8* at EKL1 motif sites, prompted us to investigate crosstalk between *CHD8* and *ELK1* in transcription, using image-based analysis of nuclear ELK1 binding. We sought to modulate distinct transcription stage in CHD8 KO cells and measure the punctate-ELK1 on the nucleus (31) (Fig. 5a). In rat cortical neurons, ELK1 is located mostly in the cytosol, whereas upon an increase in intracellular calcium influx or stimulation of the glutamate receptor, it localizes to the nucleus (32). Indeed our immunostaining in human neurons revealed ELK1 is present at both nucleus and cytoplasm, but the number of punctate nuclear decreases upon treatment of cells with transcription inhibitors (Fig. 5b). We hypothesized spatial organization of ELK1 punctate depends on cellular transcriptional activity, and CHD8 plays a role in facilitating the

interaction of ELK1 with its genomic targets and for the organization of ELK1 punctate. Therefore we modulated transcription by directly inhibiting RNA polymerase (Pol) II activity at initiation or elongation using previously discovered chemical inhibitors. One of these molecules, cyclin-dependent kinase inhibitor, preventing elongation step, and Triptolide (TPL), significantly decreases transcription initiation by direct inhibition of Pol II subunits (33-36) (Fig. 5a, b). CHD8 KO and control neurons treated with the small molecules, and after 30 minutes, cells were fixed and immunostained with the ELK1 antibody. We compared the counts of ELK1 puncta from a particular genotype, stained for Cre or ΔCre-GFP, to a non-infected cell within the same coverslip to avoid non-specific signal artifacts arising from variable florescent signal adjustments. The result showed CHD8 KO causes a decrease in ELK1 puncta in the condition of inhibiting transcription elongation (Flavopiridol treatment). We found no significant change in ELK1 staining at CHD8 KO cells when transcription initiation was blocked. Therefore, CHD8 KO led to disturbance and decrease in nuclear ELK1 localization, in transcription- depended manner.

To identify additional ETS factors that might functionally interact with CHD8, we turned to our gene expression from wild type neurons. We found that ELK1 is the only highly expressed ETS factor in human neurons (Extended Data Fig. 11e) (37). Therefore, we constructed lentiviral vectors carrying short hairpin RNA (shRNA) sequences targeting *ELK1* and also *ELF4* gene as a control to validate that ELK1 is the only ETS factor that functionally interacts with CHD8. Quantitative qPCR and western blotting confirmed a robust decrease in mRNA and protein after infection with two different hairpins against *ELK1* and one hairpin against *ELF4* (Extended Data Fig. 11e). To investigate the potential functional cooperation between *ELK1* and *CHD8 on* chromatin binding we knockdown *ELK1* by shRNA and we measured the binding of CHD8 at a series of CHD8 binding peak regions with ChIP-qPCR. The selected peaks that we validated from three independent pull-down experiments showed compelete absence of CHD8 binding in KO neurons (Extended Data Fig. 11a-b). As a control, we knockdown another ETS factor-*ELF4* and assessed the binding of CHD8 (Extended Data Fig. 11d). Results showed when *ELK1* is knockdown in neurons, CHD8 peaks that contained ETS motifs were strongly decreased, whereas CHD8 sites without ETS motifs were unaffected (Fig. 5c). ELF4 knockdown did not change CHD8 binding at the same peak sites (Extended Data Fig. 11d). Thus, ELK1 is the critical ETS factor that is necessary for the proper chromatin interaction and targeting of CHD8.

Discussion

While there are many epigenetic regulators required for the establishment of pluripotency and for exit from the pluripotent state, only a few of them are also needed for cellular maintenance of established pluripotent stem cell lines (39). It is; therefore, remarkable that CHD8 is essential for pluripotent stem cell survival. Due to the early embryonic lethality of *CHD8* KO mice, its molecular function has been difficult to study (40). Past studies show that heterozygous *CHD8* deletions recapitulate some aspects of human syndrome (41-45). However, results from a recently published comprehensive study show, at all the current heterozygous CHD8 knockout models across the publication, the mRNA does not uniformly decrease to 50% of wild type expression. Indeed, a few of the knockdown models resulted in up to 20% decrease. Still many did not drop down to even 60% of wild type expression, suggesting there is extremely high variability across the models (16). These observations led us to hypothesize that the inducible, homozygous knockout model is the best representative of CHD8 loss for functional studies (16). Furthermore, we observed many of the proposed functional pathways in autism gene modules are transcription or chromatin factors and; therefore, highly dosage-sensitive (46-48). Consequently, inadequate perturbation of CHD8 could lead to an inaccurate effect in prominent downstream targets and cause misinterpretations.

Another essential task in modeling autism is to capture the phenotypic specificity in the accurate cell type. Autism is a condition primarily associated with brain dysfunction(49). Despite the heterogeneity of autism phenotype, there are distinct behavioral phenotypes common among all cases, and CHD8 leads to one of the most reproducible ASD phenotypes (50). Conversely, The brain is the organ with the most diverse cell types throughout the body; therefore, modeling autism should capture phenotypic specificity in the accurate cell type(51, 52). The ASD phenotype`s cell-type specificity revealed in findings from a single-cell gene expression study, at which distinct cell-type appeared among the Go terms in ASD brain. The cell-type-specific Go terms did not belong to glia, microglia, endothelial, or oligodendrocyte cells, but they were distinctly related to neurons and synapse function (53). Most importantly, the clinical severity score of ASD is highly correlated with the number of neuron-specific DEGs from the same patient. Therefore, we hypothesize modeling CHD8 mutation in neurons is the most accurate predictor of ASD related pathology.

Our conditional KO approach allowed us to overcome the following limitations and also the problem of an early developmental lethality, to interrogate CHD8's cellular function in defined cell types.

Overall our results showed mutant human postmitotic neurons showed no survival deficit in stark contrast to pluripotent cells. Instead, we found compelling evidence that CHD8 is a chromatin

remodeler that promotes the formation of accessible chromatin and transcriptional activation at its genomic targets, including ASD genes and prominent chromatin remodeling factors.

Another insight of the current study is that proper chromatin targeting of CHD8 requires ELK1 specifically at ETS motif-containing sites and functional interaction between the two factors regulating neurogenesis of pluripotent stem cells. ELK1 is known to be primarily a transcriptional activator (26) which is well compatible with our finding that CHD8 promotes chromatin accessibility and transcription at ELK1 sites. The well-characterized direct phosphorylation of ELK1 by MAP kinases, including ERK is also needed to mediate CHD8 function as pharmacological MAPK inhibition mimicked the effects of ELK1 loss-of-function (54). In light of these data, it is intriguing to speculate that MAPK/ERK/ELK1 may play a functional role in developing neuropsychiatric alterations caused by *CHD8* mutations. Modulation of specific aspects of this pathway, which is known to regulate activity-dependent gene expression and synaptic plasticity (55, 56), may represent a foundation to explore a therapeutic opportunity for functional interference with pathology induced by *CHD8* mutations.

BIBLIOGRAPHY

1. Sanders SJ, Murtha MT, Gupta AR, Murdoch JD, Raubeson MJ, Willsey AJ, Ercan-Sencicek AG, DiLullo NM, Parikshak NN, Stein JL, Walker MF, Ober GT, Teran NA, Song Y, El-Fishawy P, Murtha RC, Choi M, Overton JD, Bjornson RD, Carriero NJ, Meyer KA, Bilguvar K, Mane SM, Sestan N, Lifton RP, Gunel M, Roeder K, Geschwind DH, Devlin B, State MW. De novo mutations revealed by whole-exome sequencing are strongly associated with autism. Nature. 2012;485(7397):237-41. Epub 2012/04/13. doi: 10.1038/nature10945. PubMed PMID: 22495306; PubMed Central PMCID: PMCPmc3667984.
2. O'Roak BJ, Vives L, Fu W, Egertson JD, Stanaway IB, Phelps IG, Carvill G, Kumar A, Lee C, Ankenman K, Munson J, Hiatt JB, Turner EH, Levy R, O'Day DR, Krumm N, Coe BP, Martin BK, Borenstein E, Nickerson DA, Mefford HC, Doherty D, Akey JM, Bernier R, Eichler EE, Shendure J. Multiplex targeted sequencing identifies recurrently mutated genes in autism spectrum disorders. Science. 2012;338(6114):1619-22. Epub 2012/11/20. doi: 10.1126/science.1227764. PubMed PMID: 23160955; PubMed Central PMCID: PMCPmc3528801.
3. O'Roak BJ, Vives L, Girirajan S, Karakoc E, Krumm N, Coe BP, Levy R, Ko A, Lee C, Smith JD, Turner EH, Stanaway IB, Vernot B, Malig M, Baker C, Reilly B, Akey JM, Borenstein E, Rieder MJ, Nickerson DA, Bernier R, Shendure J, Eichler EE. Sporadic autism exomes reveal a highly interconnected protein network of de novo mutations. Nature. 2012;485(7397):246-50. Epub 2012/04/13. doi: 10.1038/nature10989. PubMed PMID: 22495309; PubMed Central PMCID: PMC3350576.
4. Neale BM, Kou Y, Liu L, Ma'ayan A, Samocha KE, Sabo A, Lin CF, Stevens C, Wang LS, Makarov V, Polak P, Yoon S, Maguire J, Crawford EL, Campbell NG, Geller ET, Valladares O, Schafer C, Liu H, Zhao T, Cai G, Lihm J, Dannenfelser R, Jabado O, Peralta Z, Nagaswamy U, Muzny D, Reid JG, Newsham I, Wu Y, Lewis L, Han Y, Voight BF, Lim E, Rossin E, Kirby A, Flannick J, Fromer M, Shakir K, Fennell T, Garimella K, Banks E, Poplin R, Gabriel S, DePristo M, Wimbish JR, Boone BE, Levy SE, Betancur C, Sunyaev S, Boerwinkle E, Buxbaum JD, Cook EH, Jr., Devlin B, Gibbs RA, Roeder K, Schellenberg GD, Sutcliffe JS, Daly MJ. Patterns and rates of exonic de novo mutations in autism spectrum disorders. Nature. 2012;485(7397):242-5. Epub 2012/04/13. doi: 10.1038/nature11011. PubMed PMID: 22495311; PubMed Central PMCID: PMC3613847.
5. Cruzalegui FH, Cano E, Treisman R. ERK activation induces phosphorylation of Elk-1 at multiple S/T-P motifs to high stoichiometry. Oncogene. 1999;18(56):7948-57. Epub 2000/01/19. doi: 10.1038/sj.onc.1203362. PubMed PMID: 10637505.
6. Zhang Y, Pak C, Han Y, Ahlenius H, Zhang Z, Chanda S, Marro S, Patzke C, Acuna C, Covy J, Xu W, Yang N, Danko T, Chen L, Wernig M, Sudhof TC. Rapid single-step induction of functional neurons from human pluripotent stem cells. Neuron. 2013;78(5):785-98. Epub 2013/06/15. doi: 10.1016/j.neuron.2013.05.029. PubMed PMID: 23764284; PubMed Central PMCID: PMCPmc3751803.
7. Liu X, Li M, Xia X, Li X, Chen Z. Mechanism of chromatin remodelling revealed by the Snf2-nucleosome structure. Nature. 2017;544(7651):440-5. Epub 2017/04/21. doi: 10.1038/nature22036. PubMed PMID: 28424519.
8. Tyler JK, Kadonaga JT. The "dark side" of chromatin remodeling: repressive effects on transcription. Cell. 1999;99(5):443-6. Epub 1999/12/10. doi: 10.1016/s0092-8674(00)81530-5. PubMed PMID: 10589670.
9. Fyodorov DV, Blower MD, Karpen GH, Kadonaga JT. Acf1 confers unique activities to ACF/CHRAC and promotes the formation rather than disruption of chromatin in vivo. Genes & development. 2004;18(2):170-83. Epub 2004/01/31. doi: 10.1101/gad.1139604. PubMed PMID: 14752009; PubMed Central PMCID: PMCPmc324423.
10. Narlikar GJ, Sundaramoorthy R, Owen-Hughes T. Mechanisms and functions of ATP-dependent chromatin-remodeling enzymes. Cell. 2013;154(3):490-503. Epub 2013/08/06. doi: 10.1016/j.cell.2013.07.011. PubMed PMID: 23911317; PubMed Central PMCID: PMCPmc3781322.

11. de Dieuleveult M, Yen K, Hmitou I, Depaux A, Boussouar F, Bou Dargham D, Jounier S, Humbertclaude H, Ribierre F, Baulard C, Farrell NP, Park B, Keime C, Carriere L, Berlivet S, Gut M, Gut I, Werner M, Deleuze JF, Olaso R, Aude JC, Chantalat S, Pugh BF, Gerard M. Genome-wide nucleosome specificity and function of chromatin remodellers in ES cells. Nature. 2016;530(7588):113-6. Epub 2016/01/28. doi: 10.1038/nature16505. PubMed PMID: 26814966; PubMed Central PMCID: PMCPmc4871117.
12. Andersson R, Gebhard C, Miguel-Escalada I, Hoof I, Bornholdt J, Boyd M, Chen Y, Zhao X, Schmidl C, Suzuki T, Ntini E, Arner E, Valen E, Li K, Schwarzfischer L, Glatz D, Raithel J, Lilje B, Rapin N, Bagger FO, Jorgensen M, Andersen PR, Bertin N, Rackham O, Burroughs AM, Baillie JK, Ishizu Y, Shimizu Y, Furuhata E, Maeda S, Negishi Y, Mungall CJ, Meehan TF, Lassmann T, Itoh M, Kawaji H, Kondo N, Kawai J, Lennartsson A, Daub CO, Heutink P, Hume DA, Jensen TH, Suzuki H, Hayashizaki Y, Muller F, Forrest ARR, Carninci P, Rehli M, Sandelin A. An atlas of active enhancers across human cell types and tissues. Nature. 2014;507(7493):455-61. Epub 2014/03/29. doi: 10.1038/nature12787. PubMed PMID: 24670763; PubMed Central PMCID: PMCPmc5215096.
13. Davis CA, Hitz BC, Sloan CA, Chan ET, Davidson JM, Gabdank I, Hilton JA, Jain K, Baymuradov UK, Narayanan AK, Onate KC, Graham K, Miyasato SR, Dreszer TR, Strattan JS, Jolanki O, Tanaka FY, Cherry JM. The Encyclopedia of DNA elements (ENCODE): data portal update. Nucleic acids research. 2018;46(D1):D794-d801. Epub 2017/11/11. doi: 10.1093/nar/gkx1081. PubMed PMID: 29126249; PubMed Central PMCID: PMCPmc5753278.
14. Jolma A, Yan J, Whitington T, Toivonen J, Nitta KR, Rastas P, Morgunova E, Enge M, Taipale M, Wei G, Palin K, Vaquerizas JM, Vincentelli R, Luscombe NM, Hughes TR, Lemaire P, Ukkonen E, Kivioja T, Taipale J. DNA-binding specificities of human transcription factors. Cell. 2013;152(1-2):327-39. Epub 2013/01/22. doi: 10.1016/j.cell.2012.12.009. PubMed PMID: 23332764.
15. Wang P, Mokhtari R, Pedrosa E, Kirschenbaum M, Bayrak C, Zheng D, Lachman HM. CRISPR/Cas9-mediated heterozygous knockout of the autism gene CHD8 and characterization of its transcriptional networks in cerebral organoids derived from iPS cells. Molecular autism. 2017;8:11. Epub 2017/03/23. doi: 10.1186/s13229-017-0124-1. PubMed PMID: 28321286; PubMed Central PMCID: PMCPmc5357816.
16. Wade AA, Lim K, Catta-Preta R, Nord AS. Common CHD8 Genomic Targets Contrast With Model-Specific Transcriptional Impacts of CHD8 Haploinsufficiency. Frontiers in molecular neuroscience. 2018;11:481. Epub 2019/01/30. doi: 10.3389/fnmol.2018.00481. PubMed PMID: 30692911; PubMed Central PMCID: PMCPmc6339895.
17. Gupta S, Ellis SE, Ashar FN, Moes A, Bader JS, Zhan J, West AB, Arking DE. Transcriptome analysis reveals dysregulation of innate immune response genes and neuronal activity-dependent genes in autism. Nature communications. 2014;5:5748. Epub 2014/12/11. doi: 10.1038/ncomms6748. PubMed PMID: 25494366; PubMed Central PMCID: PMCPmc4270294.
18. Abrahams BS, Arking DE, Campbell DB, Mefford HC, Morrow EM, Weiss LA, Menashe I, Wadkins T, Banerjee-Basu S, Packer A. SFARI Gene 2.0: a community-driven knowledgebase for the autism spectrum disorders (ASDs). Molecular autism. 2013;4(1):36. Epub 2013/10/05. doi: 10.1186/2040-2392-4-36. PubMed PMID: 24090431; PubMed Central PMCID: PMCPmc3851189.
19. Voineagu I, Wang X, Johnston P, Lowe JK, Tian Y, Horvath S, Mill J, Cantor RM, Blencowe BJ, Geschwind DH. Transcriptomic analysis of autistic brain reveals convergent molecular pathology. Nature. 2011;474(7351):380-4. Epub 2011/05/27. doi: 10.1038/nature10110. PubMed PMID: 21614001; PubMed Central PMCID: PMCPmc3607626.
20. De Rubeis S, He X, Goldberg AP, Poultney CS, Samocha K, Cicek AE, Kou Y, Liu L, Fromer M, Walker S, Singh T, Klei L, Kosmicki J, Shih-Chen F, Aleksic B, Biscaldi M, Bolton PF, Brownfeld JM, Cai J, Campbell NG, Carracedo A, Chahrour MH, Chiocchetti AG, Coon H, Crawford EL, Curran SR, Dawson G, Duketis E, Fernandez BA, Gallagher L, Geller E, Guter SJ, Hill RS, Ionita-Laza J, Jimenz Gonzalez P, Kilpinen H, Klauck SM, Kolevzon A, Lee I, Lei I, Lei J, Lehtimäki T, Lin CF, Ma'ayan A, Marshall CR, McInnes AL, Neale B, Owen MJ, Ozaki N, Parellada M, Parr JR, Purcell S, Puura K, Rajagopalan D, Rehnström K, Reichenberg A, Sabo A, Sachse M, Sanders SJ, Schafer C, Schulte-Rüther M, Skuse D, Stevens C, Szatmari P, Tammimies K, Valladares O, Voran A, Li-San W,

Weiss LA, Willsey AJ, Yu TW, Yuen RK, Cook EH, Freitag CM, Gill M, Hultman CM, Lehner T, Palotie A, Schellenberg GD, Sklar P, State MW, Sutcliffe JS, Walsh CA, Scherer SW, Zwick ME, Barett JC, Cutler DJ, Roeder K, Devlin B, Daly MJ, Buxbaum JD. Synaptic, transcriptional and chromatin genes disrupted in autism. Nature. 2014;515(7526):209-15. Epub 2014/11/05. doi: 10.1038/nature13772. PubMed PMID: 25363760; PubMed Central PMCID: PMCPmc4402723.
21. Buenrostro JD, Giresi PG, Zaba LC, Chang HY, Greenleaf WJ. Transposition of native chromatin for fast and sensitive epigenomic profiling of open chromatin, DNA-binding proteins and nucleosome position. Nature methods. 2013;10(12):1213-8. Epub 2013/10/08. doi: 10.1038/nmeth.2688. PubMed PMID: 24097267; PubMed Central PMCID: PMCPmc3959825.
22. Schep AN, Buenrostro JD, Denny SK, Schwartz K, Sherlock G, Greenleaf WJ. Structured nucleosome fingerprints enable high-resolution mapping of chromatin architecture within regulatory regions. Genome research. 2015;25(11):1757-70. Epub 2015/09/01. doi: 10.1101/gr.192294.115. PubMed PMID: 26314830; PubMed Central PMCID: PMCPmc4617971.
23. Doan RN, Lim ET, De Rubeis S, Betancur C, Cutler DJ, Chiocchetti AG, Overman LM, Soucy A, Goetze S, Freitag CM, Daly MJ, Walsh CA, Buxbaum JD, Yu TW. Recessive gene disruptions in autism spectrum disorder. Nature genetics. 2019;51(7):1092-8. Epub 2019/06/19. doi: 10.1038/s41588-019-0433-8. PubMed PMID: 31209396; PubMed Central PMCID: PMCPmc6629034.
24. An integrated encyclopedia of DNA elements in the human genome. Nature. 2012;489(7414):57-74. Epub 2012/09/08. doi: 10.1038/nature11247. PubMed PMID: 22955616; PubMed Central PMCID: PMCPmc3439153.
25. Ernst J, Kellis M. Chromatin-state discovery and genome annotation with ChromHMM. Nature protocols. 2017;12(12):2478-92. Epub 2017/11/10. doi: 10.1038/nprot.2017.124. PubMed PMID: 29120462; PubMed Central PMCID: PMCPmc5945550.
26. Besnard A, Galan-Rodriguez B, Vanhoutte P, Caboche J. Elk-1 a transcription factor with multiple facets in the brain. Frontiers in neuroscience. 2011;5:35. Epub 2011/03/29. doi: 10.3389/fnins.2011.00035. PubMed PMID: 21441990; PubMed Central PMCID: PMCPmc3060702.
27. Vickers ER, Kasza A, Kurnaz IA, Seifert A, Zeef LA, O'Donnell A, Hayes A, Sharrocks AD. Ternary complex factor-serum response factor complex-regulated gene activity is required for cellular proliferation and inhibition of apoptotic cell death. Molecular and cellular biology. 2004;24(23):10340-51. Epub 2004/11/16. doi: 10.1128/mcb.24.23.10340-10351.2004. PubMed PMID: 15542842; PubMed Central PMCID: PMCPmc529045.
28. Stevens JL, Cantin GT, Wang G, Shevchenko A, Shevchenko A, Berk AJ. Transcription control by E1A and MAP kinase pathway via Sur2 mediator subunit. Science (New York, NY). 2002;296(5568):755-8. Epub 2002/04/06. doi: 10.1126/science.1068943. PubMed PMID: 11934987.
29. Wang G, Balamotis MA, Stevens JL, Yamaguchi Y, Handa H, Berk AJ. Mediator requirement for both recruitment and postrecruitment steps in transcription initiation. Molecular cell. 2005;17(5):683-94. Epub 2005/03/08. doi: 10.1016/j.molcel.2005.02.010. PubMed PMID: 15749018.
30. Balamotis MA, Pennella MA, Stevens JL, Wasylyk B, Belmont AS, Berk AJ. Complexity in transcription control at the activation domain-mediator interface. Science signaling. 2009;2(69):ra20. Epub 2009/05/07. doi: 10.1126/scisignal.1164302. PubMed PMID: 19417216; PubMed Central PMCID: PMCPmc2774526.
31. Zhang HM, Li L, Papadopoulou N, Hodgson G, Evans E, Galbraith M, Dear M, Vougier S, Saxton J, Shaw PE. Mitogen-induced recruitment of ERK and MSK to SRE promoter complexes by ternary complex factor Elk-1. Nucleic acids research. 2008;36(8):2594-607. Epub 2008/03/13. doi: 10.1093/nar/gkn099. PubMed PMID: 18334532; PubMed Central PMCID: PMCPmc2377423.
32. Sgambato V, Vanhoutte P, Pagès C, Rogard M, Hipskind R, Besson MJ, Caboche J. In vivo expression and regulation of Elk-1, a target of the extracellular-regulated kinase signaling pathway, in the adult rat brain. The Journal of neuroscience : the official journal of the Society for Neuroscience. 1998;18(1):214-26. Epub 1998/01/24. doi: 10.1523/jneurosci.18-01-00214.1998. PubMed PMID: 9412502; PubMed Central PMCID: PMCPmc6793414.

33. Sedlacek HH. Mechanisms of action of flavopiridol. Critical reviews in oncology/hematology. 2001;38(2):139-70. Epub 2001/04/20. doi: 10.1016/s1040-8428(00)00124-4. PubMed PMID: 11311660.
34. Chen F, Gao X, Shilatifard A. Stably paused genes revealed through inhibition of transcription initiation by the TFIIH inhibitor triptolide. Genes & development. 2015;29(1):39-47. Epub 2015/01/07. doi: 10.1101/gad.246173.114. PubMed PMID: 25561494; PubMed Central PMCID: PMCPmc4281563.
35. Vispé S, DeVries L, Créancier L, Besse J, Bréand S, Hobson DJ, Svejstrup JQ, Annereau JP, Cussac D, Dumontet C, Guilbaud N, Barret JM, Bailly C. Triptolide is an inhibitor of RNA polymerase I and II-dependent transcription leading predominantly to down-regulation of short-lived mRNA. Molecular cancer therapeutics. 2009;8(10):2780-90. Epub 2009/10/08. doi: 10.1158/1535-7163.mct-09-0549. PubMed PMID: 19808979.
36. Titov DV, Gilman B, He QL, Bhat S, Low WK, Dang Y, Smeaton M, Demain AL, Miller PS, Kugel JF, Goodrich JA, Liu JO. XPB, a subunit of TFIIH, is a target of the natural product triptolide. Nature chemical biology. 2011;7(3):182-8. Epub 2011/02/01. doi: 10.1038/nchembio.522. PubMed PMID: 21278739; PubMed Central PMCID: PMCPmc3622543.
37. Maroulakou IG, Bowe DB. Expression and function of Ets transcription factors in mammalian development: a regulatory network. Oncogene. 2000;19(55):6432-42. Epub 2001/02/15. doi: 10.1038/sj.onc.1204039. PubMed PMID: 11175359.
38. Qi Y, Zhang XJ, Renier N, Wu Z, Atkin T, Sun Z, Ozair MZ, Tchieu J, Zimmer B, Fattahi F, Ganat Y, Azevedo R, Zeltner N, Brivanlou AH, Karayiorgou M, Gogos J, Tomishima M, Tessier-Lavigne M, Shi SH, Studer L. Combined small-molecule inhibition accelerates the derivation of functional cortical neurons from human pluripotent stem cells. Nature biotechnology. 2017;35(2):154-63. Epub 2017/01/24. doi: 10.1038/nbt.3777. PubMed PMID: 28112759; PubMed Central PMCID: PMCPmc5516899.
39. Surani MA, Hayashi K, Hajkova P. Genetic and epigenetic regulators of pluripotency. Cell. 2007;128(4):747-62. Epub 2007/02/27. doi: 10.1016/j.cell.2007.02.010. PubMed PMID: 17320511.
40. Nishiyama M, Oshikawa K, Tsukada Y, Nakagawa T, Iemura S, Natsume T, Fan Y, Kikuchi A, Skoultchi AI, Nakayama KI. CHD8 suppresses p53-mediated apoptosis through histone H1 recruitment during early embryogenesis. Nature cell biology. 2009;11(2):172-82. Epub 2009/01/20. doi: 10.1038/ncb1831. PubMed PMID: 19151705; PubMed Central PMCID: PMCPmc3132516.
41. Sugathan A, Biagioli M, Golzio C, Erdin S, Blumenthal I, Manavalan P, Ragavendran A, Brand H, Lucente D, Miles J, Sheridan SD, Stortchevoi A, Kellis M, Haggarty SJ, Katsanis N, Gusella JF, Talkowski ME. CHD8 regulates neurodevelopmental pathways associated with autism spectrum disorder in neural progenitors. Proc Natl Acad Sci U S A. 2014;111(42):E4468-77. Epub 2014/10/09. doi: 10.1073/pnas.1405266111. PubMed PMID: 25294932; PubMed Central PMCID: PMCPmc4210312.
42. Gompers AL, Su-Feher L, Ellegood J, Copping NA, Riyadh MA, Stradleigh TW, Pride MC, Schaffler MD, Wade AA, Catta-Preta R, Zdilar I, Louis S, Kaushik G, Mannion BJ, Plajzer-Frick I, Afzal V, Visel A, Pennacchio LA, Dickel DE, Lerch JP, Crawley JN, Zarbalis KS, Silverman JL, Nord AS. Germline Chd8 haploinsufficiency alters brain development in mouse. Nature neuroscience. 2017;20(8):1062-73. Epub 2017/07/04. doi: 10.1038/nn.4592. PubMed PMID: 28671691; PubMed Central PMCID: PMCPmc6008102.
43. Platt RJ, Zhou Y, Slaymaker IM, Shetty AS, Weisbach NR, Kim JA, Sharma J, Desai M, Sood S, Kempton HR, Crabtree GR, Feng G, Zhang F. Chd8 Mutation Leads to Autistic-like Behaviors and Impaired Striatal Circuits. Cell reports. 2017;19(2):335-50. Epub 2017/04/14. doi: 10.1016/j.celrep.2017.03.052. PubMed PMID: 28402856; PubMed Central PMCID: PMCPmc5455342.
44. Katayama Y, Nishiyama M, Shoji H, Ohkawa Y, Kawamura A, Sato T, Suyama M, Takumi T, Miyakawa T, Nakayama KI. CHD8 haploinsufficiency results in autistic-like phenotypes in mice. Nature. 2016;537(7622):675-9. Epub 2016/09/08. doi: 10.1038/nature19357. PubMed PMID: 27602517.

45. Durak O, Gao F, Kaeser-Woo YJ, Rueda R, Martorell AJ, Nott A, Liu CY, Watson LA, Tsai LH. Chd8 mediates cortical neurogenesis via transcriptional regulation of cell cycle and Wnt signaling. Nature neuroscience. 2016;19(11):1477-88. Epub 2016/10/28. doi: 10.1038/nn.4400. PubMed PMID: 27694995; PubMed Central PMCID: PMCPmc5386887.
46. Takeuchi JK, Lou X, Alexander JM, Sugizaki H, Delgado-Olguín P, Holloway AK, Mori AD, Wylie JN, Munson C, Zhu Y, Zhou YQ, Yeh RF, Henkelman RM, Harvey RP, Metzger D, Chambon P, Stainier DY, Pollard KS, Scott IC, Bruneau BG. Chromatin remodelling complex dosage modulates transcription factor function in heart development. Nature communications. 2011;2:187. Epub 2011/02/10. doi: 10.1038/ncomms1187. PubMed PMID: 21304516; PubMed Central PMCID: PMCPmc3096875.
47. Kadoch C, Crabtree GR. Mammalian SWI/SNF chromatin remodeling complexes and cancer: Mechanistic insights gained from human genomics. Science advances. 2015;1(5):e1500447. Epub 2015/11/26. doi: 10.1126/sciadv.1500447. PubMed PMID: 26601204; PubMed Central PMCID: PMCPmc4640607.
48. Krumm N, O'Roak BJ, Shendure J, Eichler EE. A de novo convergence of autism genetics and molecular neuroscience. Trends in neurosciences. 2014;37(2):95-105. Epub 2014/01/07. doi: 10.1016/j.tins.2013.11.005. PubMed PMID: 24387789; PubMed Central PMCID: PMCPmc4077788.
49. Minshew NJ, Keller TA. The nature of brain dysfunction in autism: functional brain imaging studies. Current opinion in neurology. 2010;23(2):124-30. Epub 2010/02/16. doi: 10.1097/WCO.0b013e32833782d4. PubMed PMID: 20154614; PubMed Central PMCID: PMCPmc2975255.
50. Barnard RA, Pomaville MB, O'Roak BJ. Mutations and Modeling of the Chromatin Remodeler CHD8 Define an Emerging Autism Etiology. Frontiers in neuroscience. 2015;9:477. Epub 2016/01/07. doi: 10.3389/fnins.2015.00477. PubMed PMID: 26733790; PubMed Central PMCID: PMCPmc4681771.
51. Mayer S, Chen J, Velmeshev D, Mayer A, Eze UC, Bhaduri A, Cunha CE, Jung D, Arjun A, Li E, Alvarado B, Wang S, Lovegren N, Gonzales ML, Szpankowski L, Leyrat A, West JAA, Panagiotakos G, Alvarez-Buylla A, Paredes MF, Nowakowski TJ, Pollen AA, Kriegstein AR. Multimodal Single-Cell Analysis Reveals Physiological Maturation in the Developing Human Neocortex. Neuron. 2019;102(1):143-58.e7. Epub 2019/02/17. doi: 10.1016/j.neuron.2019.01.027. PubMed PMID: 30770253.
52. Zhong S, Zhang S, Fan X, Wu Q, Yan L, Dong J, Zhang H, Li L, Sun L, Pan N, Xu X, Tang F, Zhang J, Qiao J, Wang X. A single-cell RNA-seq survey of the developmental landscape of the human prefrontal cortex. Nature. 2018;555(7697):524-8. Epub 2018/03/15. doi: 10.1038/nature25980. PubMed PMID: 29539641.
53. Velmeshev D, Schirmer L, Jung D, Haeussler M, Perez Y, Mayer S, Bhaduri A, Goyal N, Rowitch DH, Kriegstein AR. Single-cell genomics identifies cell type-specific molecular changes in autism. Science (New York, NY). 2019;364(6441):685-9. Epub 2019/05/18. doi: 10.1126/science.aav8130. PubMed PMID: 31097668.
54. Yang SH, Yates PR, Whitmarsh AJ, Davis RJ, Sharrocks AD. The Elk-1 ETS-domain transcription factor contains a mitogen-activated protein kinase targeting motif. Molecular and cellular biology. 1998;18(2):710-20. Epub 1998/02/03. doi: 10.1128/mcb.18.2.710. PubMed PMID: 9447967; PubMed Central PMCID: PMCPmc108782.
55. Dolmetsch RE, Pajvani U, Fife K, Spotts JM, Greenberg ME. Signaling to the nucleus by an L-type calcium channel-calmodulin complex through the MAP kinase pathway. Science. 2001;294(5541):333-9. Epub 2001/10/13. doi: 10.1126/science.1063395. PubMed PMID: 11598293.
56. Thomas GM, Huganir RL. MAPK cascade signalling and synaptic plasticity. Nature reviews Neuroscience. 2004;5(3):173-83. Epub 2004/02/21. doi: 10.1038/nrn1346. PubMed PMID: 14976517.

METHODS

Cell culture. CHD8-KO human ES cells were generated from the human embryonic stem cell (ESC) line H9 (passage 50, WA09 WiCell Research Institute, Inc.) and an iPSC line from a male individual (karyotype is shown in Figure S2-1). Only cells with normal karyotype were used to generate conditional knockout cells and downstream analysis. Pluripotent stem cells were maintained in mTeSR1 (STEMCELL Technologies) and small-molecule Thiazovivin (5μM) (STEMCELL Technologies) applied to the medium before single cell passaging. The conversion of PSC to induced neurons is described below according to our previously published protocol [1].

Lentivirus generation. Production of lentivirus was according to the previously described method [2].

Production of Adeno-Associated Virus (AAV). Recombinant adeno-associated virus (rAAV-DJ) was used to deliver the targeting vector to pluripotent stem cells. To produce rAAV we co-transfected three plasmids: 25 μg of pAAV [3], 25 μg of helper plasmid (pAd5) and 20 μg of capsid (AAV-DJ), into one T75 flask with 80% confluent HEK293T cells (ATCC) by calcium phosphate transfection method [3,4]. Two days after transfection, cells were harvested by trypsin for 10 minutes and lysed by three rounds of freeze and thawing in dry ice and water bath (37□C). The rAAV virus was collected from the supernatant by spinning the whole lysate and removal of the pellet. The virus was aliquoted in small volumes to freeze in -80ºC. Before usage for every 100 μl of supernatant, ten units of Benzonase endonuclease (EMD Chemical Inc, Merck 1.01695.002) added at (37ºC) for 5 minutes to digest DNA from HEK cells; the capsid protects AAV DNA from digestion.

Generation of human induced excitatory neurons (iN). Human excitatory neurons differentiated from pluripotent stem cells by over-expression of lineage-specific transcription factor-Neurogenin 2 (Ngn2) as described before[1]. In summary, one day prior to conversion, we dissociated stem cells into single cells with Accutase (Innovative Cell Technologies) and seeded at ~ 40K cells into one 24 well plate pre-coated with Matrigel (BD Biosciences) in medium supplemented with Thiazovivin (5μM) (STEMCELL Technologies) and doxycycline (2 mg/ml, Clontech). After 6 hours, we infected the cells with lentivirus containing Ngn2, RTTA, and Cre recombinase or ΔCre (truncated form of Cre which is not functional and it is used as control). The next day we replaced the medium with neuronal medium N2/DMEM/F12/NEAA (Invitrogen) containing doxycycline (2 mg/ml, Clontech). We kept the cells in this medium for 5 days, and on day 6 we added ~ 10K mouse glia cells into each 24 well and replaced the culture medium with serum-containing medium. We analyzed the cultures approximately

3-5 weeks after induction. To generate homozygous knockout neurons, we infected the neurons with LV- Cre or ΔCre one day after induction of the Ngn2 transcription factor.

Immunofluorescence (IF). For immunofluorescence (IF) staining of cells (embryonic stem cells and iN cells) we fixed the cells using 4% paraformaldehyde (PFA) for 15 minutes at room temperature and permeabilized the cell membrane using 5% Triton for 1 hour and then blocked the cells in a solution containing 1% BSA, 5% FBS and 1%Triton. The primary antibody was added to the same blocking buffer according to these dilutions: CHD8 antibody (Rabbit-Behtyl lab-A301-224A) used as 1:3,000, Synapsin1 antibody (Rabbit- Synaptic Systems-106002) used as 1:500, Homer1 (Rabbit-Synaptic Systems-160003) used as 1:500, HA (Rabbit-Sigma-H6908) used as 1:500, Map2 (Mouse-Sigma-M9942) used as 1:500,Tuj1 (Rabbit-Biolegened-802001) used as 1:500, ELK1 (Rabbit, Bethyl lab-A303-529A) used as 1:400 and incubated for O/N at 4ºC. DAPI added as 100 nM solution for 1 minute. The secondary antibodies were made as 1:1,000 solutions and incubated for 1hr at room temperature.

Western blotting. Human stem cells and neurons lysed with RIPA lysis buffer supplemented with 5mM EDTA and protease inhibitor (Roche), for 5 minutes at room temperature and 10 minutes on ice. After the lysis, sample buffer (4x Laemmli buffer containing 4% SDS, 10% 2-mecaptaneol, 20% glycerol, 0.004% 4-Bromophenol blue, 0.125 M Tris HCl, pH 6.8) added and the samples either directly loaded on 4-12% SDS-PAGE gel, or froze in -80 for further analysis. For all of the immunoblots, approximately 20 to 30 µg protein was separated on an SDS-PAGE gel. Antibodies used in this manuscript used with this dilutions: CHD8 antibody (Rabbit-Behtyl lab-A301-224A) used as 1:4,000, ELK1 (Rabbit, Bethyl lab-A303-529A) used as 1:1,000, HA (Rabbit-Sigma-H6908) used as 1:1,000, β-actin antibody (Rabbit,Abcam-ab8227) used as 1:20,000. All blots visualized by fluorescently labeled secondary antibodies on Odyssey CLx Infrared Imager with Odyssey software (LI-COR Biosciences).

RNA-sequencing. RNA was obtained from 3 weeks-old cultures of iN cells by adding Trizol LS (Thermo Fisher Scientific) directly into cell culture well. Total 500 ng RNA processed for library preparation using “TruSeq” RNA sample preparation-V2 kit and “Ribo-Zero” rRNA removal kit (Illumina) according to manufacturer’s instruction. The sequencing ran on Illumina`s NextSeq 550 system with 1x 75-bp cycle run.

RNA-seq data analysis. FastQ files were run on FastQC to obtain high quality (trimmed and cleaned) reads. The reads were aligned to human reference genome sequence (hg19) and

assembled with TopHat/Bowtie (version 2.1.1)[5] for transcriptome analysis. Since we generated the library from a mix of mouse and human RNA, the resulting reads were also from a mixture of both species. We therefore aligned our reads to the human genome with stringent criteria (zero mismatches allowed). The aligned sequences randomly sampled and re-aligned to genome of the other specie (the mouse, mm9 genome) to ensure that cross-species DNA alignment is not happening. Note that ~ 1% of the reads that aligned to both human and mouse genome were discarded from SAM file with SAMtools [6]. The Refseq hg19 GTF file of transcriptome annotation was downloaded from Ensembl (https://uswest.ensembl.org/index.html) and used as a reference annotation file in TopHat alignment run command, to increase the speed and the sensitivity of alignments to splice junctions. Duplicate reads (which arise from PCR step during library preparation) were removed with SAMtools. Pre-built indexes of bowtie were downloaded from "Bowtie" webpage (http://bowtie-bio.sourceforge.net/tutorial.shtml). SAMtools subcommands were used to convert SAM files to BAM files (Bindery Alignment Map). Additionally, SAMtools were used for indexing (to view the signal on genome browser) and for sorting (necessary for downstream analysis). Cufflinks was used for transcript assembly and to estimate the abundance (FPKM) of coding genes. For quantification of transcripts across all the samples and to obtain estimated counts for downstream analysis, we used HTSeq (htseq-count option) [7]. These raw counts used as input for DESeq2 to perform differential expression analysis [8] and to generate summarizing plots.

Chromatin immunoprecipitation sequencing (ChIP-seq) and data analysis. ChIP-seq was performed with modifications from a published protocol [9]. In summary, ten confluent 10cm plates of iN cells (approximately $10x10^6$ neurons in total) 10 days after differentiation was used for chromatin extraction. Cultures were crosslinked with 1% Formaldehyde (Sigma) for 10 min at RT. Glycine (125mM) was added to quench and terminate the cross-linking reaction and after washing with PBS cells were scraped off the dishes and collected into a 50 mL tube. DNA samples were subjected to sonication to obtain an average fragment size of 200 to 600 bp, using Covaris (S220-Focused Ultrasonicator). After sonication, the pellets were cleared from debris by centrifugation in 4°C and the supernatant was collected for further analysis of DNA fragment size (column-purified DNA ran in 2% agarose gel to determine the size) and for DNA/protein concentration analysis. For input calculation approximately 0.5% of cross-linked chromatin separated and saved before the addition of IP antibody. For immunoprecipitation (IP) 1.5 µg anti-CHD8 or anti-HA antibody added into ChIP buffer (RIPA buffer supplemented with protease inhibitors, PMSF and 5mM EDTA) and left to rotate O/N in 4°C. At the same time protein G agarose beads (Active Motif) washed and blocked with 5% BSA in ChIP buffer and left to rotate O/N in 4°C. The next day, the antibody bound chromatin was added to protein G and rotated 5hr in 4°C. The immunoprecipitated material was washed and the IP material

was eluted from beads with elution buffer (50 mM NaCl, Tris-HCl;pH 7.5) by vortexing at 37 ^{o}C for 30min. The eluted DNA was separated from beads with spinning. For reverse cross-linking, the IP and input material was incubated in 65 ^{o}C/shaking along with RNaseA (10 ug/ul) and 5M NaCl plus proteinase K (20 ug/ul). DNA was purified on a column (Zymo Research) and processed for library preparation. NEBNext ChIP-seq library prep kit was used for library preparation. Sequencing was performed on Illumina`s NextSeq 550 system with 1x 75-bp cycle run. We obtained 18 to 20 million total reads per sample in one sequencing run.

ATAC-seq experiment: We followed Pi-ATAC-seq protocol for the transposition of homozygous knockout and control neurons [10]. In summary, the cells were fixed in culture for 5 minutes, with 1% PFA and detached from the plate with EDTA and stained for GFP, which allowed us to sort the Cre-GFP positive cells. After that, the transposition proceeded as standard ATAC-seq protocol with slight modification (extra step of reverse cross-linking performed overnight in 65C^{o}). Note that for heterozygous knockout and wild type transposition, we followed the original ATAC-seq protocol in which un-fixed nuclei is permeabilized and subjected to transposition [11].

ATAC-seq, ChIP-seq data analysis. For ChIP-seq and ATAC-seq ENCODE ChIP-seq pipline2 was used to obtain significant peaks[12,13]. For motif discovery, we used HOMER (v4.10) (http://homer.ucsd.edu/homer/). For clustering analysis, we used Cluster 3.0 [14]. Heatmaps were generated using java program-Treeview [15]. For ontology analysis, we used DAVID analytical tool [16]. To obtain estimated counts within the region of interest in ATAC-seq experiment we used FeatureCounts- a general-purpose read count tool from Rsubread package [17] and a custom GTF file with the coordinates of the overlapping ATAC-seq peak in all the samples used as input for the program. For library normalization and differential accessibility analysis, we used DESeq2. [8]. Differential accessible sites (opening and closing regions) were manually examined in UCSC Genome Browser with the 2019 update (http://genome.ucsc.edu). For enrichment analysis and generating normalized heatmaps and signal intensity plots, we used “deepTools” [18].

ChIP quantitative PCR (ChIP-qPCR) experiment. Total 5-10 ng ChIP DNA and the input was used to perform quantitative PCR experiment and to measure the levels of enrichment. All primers used are listed in
“ChIP-seq-peaks.xlsx” file (attached to GSE141085), along with the relevant information, including the closest gene and the number of the motif on the peak. For each peak site, 3 independent technical replicates (independent IP experiments) were used for qPCR analysis. We normalized the ChIP

signal over the input signal, which was less than 0.5% for total IP material. Analysis of qPCR experiment performed on the light Cycler 480II (Roche).

RNA extraction and RT-qPCR experiment for gene expression. For RT-qPCR and RNA-seq experiments we applied similar methods of RNA isolation: neurons that are differentiated on mouse glia cells for ~3 weeks were washed in PBS and then lysed with TRIzol added directly to the plate. RNA was purified with the ZYMO RESEARCH- Direct-zol kit. Human specific primers were used for amplification of desired RNA.

Analysis of dendritic arborizations. Neuronal cultures fixed at approximately 3 weeks after transgene induction with 4% PFA for 15 minutes. The primary and secondary antibodies dilutions are according to our method in "Immunofluorescence experiment". For morphological analysis and tracing neurites, we used the MetaMorph [19] software and for synaptic puncta analysis and other general image processing we used java program IMAGEJ and the relevant modules including CellProfiler 3.0 [20].

AAV-mediated gene targeting. For the generation of conditional CHD8 heterozygous knockout cell line we designed a donor vector for homologous recombination that carries two homology arms around the exon 4 of CHD8 gene and included two loxP sequences in the same direction for frameshifting mutation. A positive selection cassette (neomycin expression to confer resistance to Geneticin) included for purifying clones that carry the integrated donor cassette. The selection cassette contained a splice acceptor (SA) and a sequence for internal ribosomal entry site (IRES) attached to Neomycin resistance gene (NEO) and a polyadenylation (PA) signal. The NEO resistant clones used for screening PCR to verify the correct inserting of targeting vector in the locus (see Figure S2-2A to 2C). The PCR primers are designed to cover the region from outside the homology arm (primer # 1 and #4) to inside the cassette.
The drug resistance cassette was flanked with FRT sequence and later removed by transient expression of FlpE recombinase. For HA-FLAG tagging of CHD8 gene, the tags were inserted into the C-terminus region in the frame before the stop codon of Exon 38, together with Neomycin resistance gene (see Figure S1-1).
After infection of ES cells with recombinant AAV (rAAV-DJ) carrying ITR flanked targeting vectors, we selected the cells with Geneticin antibiotic (Gibco) for 10 days or until single colonies obtained. The resistant colonies expanded and genomic DNA extracted for downstream analysis.

Electrophysiology. Electrophysiological recordings in cultured iN cells were performed in the whole cell configuration as described previously [1,21]. Patch pipettes were pulled from borosilicate glass capillary tubes (Warner Instruments) using a PC-10 pipette puller (Narishige). The resistance of pipettes filled with intracellular solution varied between 2-4 MOhm. The standard bath solution contained (in mM): 140 NaCl, 5 KCl, 2 $CaCl_2$, 2 $MgCl_2$, 10 HEPES-NaOH pH 7.4, and 10 glucose; 300-305 mosm/l. Excitatory postsynaptic currents (EPSCs) were pharmacologically isolated with picrotoxin (50 μM) and recorded at -70mV holding potential in voltage-clamp mode with a pipette solution containing (in mM): 135 CsCl, 10 HEPES-CsOH pH 7.2, 5 EGTA, 4 MgATP, 0.3 Na_4GTP, and 5 QX-314; 295-300 mosm/l. Evoked EPSCs were triggered by 0.5-ms current (100 μA) injection through a local extracellular electrode (FHC concentric bipolar electrode, Catalogue number CBAEC75) placed 100–150μm from the soma of neurons recorded. The frequency, duration, and magnitude of the extracellular stimulus were controlled with a Model 2100 Isolated Pulse Stimulator (A-M Systems, Inc.) synchronized with the Clampex 9 data acquisition software (Molecular Devices). Spontaneous miniature EPSCs (mEPSCs) were monitored in the presence of tetrodotoxin (TTX, 1 μM). mEPSC events were analyzed with Clampfit 9.02 (Molecular Devices) using the template matching search and a minimal threshold of 5pA and each event was visually inspected for inclusion or rejection.Intrinsic action potential (AP) firing properties of iN cells were recorded in current-clamp mode using a pipette solution that contained (in mM): 123 K-gluconate, 10 KCl, 7 NaCl, 1 $MgCl_2$, 10 HEPES-KOH pH 7.2, 1 EGTA, 0.1 $CaCl_2$, 1.5 MgATP, 0.2 Na_4GTP and 4 glucose; 295-300 mosm/l. First, minimal currents were introduced to hold membrane potential around −70 mV, next, increasing amount of currents (from -10 pA to +60 pA, 5 pA increments) were injected for 1s in a stepwise manner to elicit action potentials. Input resistance (R_{in}) was calculated as the slope of the linear fit of the current-voltage plot generated from a series of small subthreshold current injections. To determine whole-cell membrane capacitance, square wave voltage stimulation was used to produce a pair of decaying exponential current transients that were each analyzed using a least-squares fit technique (Clampfit 9.02). Neuronal excitability recordings were performed using standard bath solution supplemented with 20 μM CNQX, 50 μM AP5 and 50 μM PTX to block all possible glutamatergic (AMPAR- and NMDAR-mediated), as well as GABAergic synaptic transmission. Drugs were applied to the bath solutions prior to all recordings. Data were digitized at 10 kHz with a 2 kHz low-pass filter using a Multiclamp 700A amplifier (Molecular Devices). For all electrophysiological experiments, the experimenter was blind to the condition/genotype of the cultures analyzed. All experiments were performed at room temperature.

Quantifications and statistical analysis

All data are shown as means +-SEM and from a minimum of three biological replicates (independent differentiations). GraphPad Prism and R were used for statistical analysis and calculations of significance.

Data and code availability

The raw sequencing files are deposited with the Gene Expression Ominibus (NCBI) (GEO accession number: GSE141085). The list of Encode data used in this study is listed in " ChIP-seq-peaks.xlsx" file (attached to GSE141085).

1 Zhang, Y. *et al.* Rapid single-step induction of functional neurons from human pluripotent stem cells. *Neuron* **78**, 785-798, doi:10.1016/j.neuron.2013.05.029 (2013).

2 Pang, Z. P. *et al.* Induction of human neuronal cells by defined transcription factors. *Nature* **476**, 220-223, doi:10.1038/nature10202 (2011).

3 Lisowski, L. *et al.* Selection and evaluation of clinically relevant AAV variants in a xenograft liver model. *Nature* **506**, 382-386, doi:10.1038/nature12875 (2014).

4 Strobel, B. *et al.* Standardized, Scalable, and Timely Flexible Adeno-Associated Virus Vector Production Using Frozen High-Density HEK-293 Cell Stocks and CELLdiscs. *Human gene therapy methods* **30**, 23-33, doi:10.1089/hgtb.2018.228 (2019).

5 Kim, D. *et al.* TopHat2: accurate alignment of transcriptomes in the presence of insertions, deletions and gene fusions. *Genome biology* **14**, R36, doi:10.1186/gb-2013-14-4-r36 (2013).

6 Li, H. *et al.* The Sequence Alignment/Map format and SAMtools. *Bioinformatics (Oxford, England)* **25**, 2078-2079, doi:10.1093/bioinformatics/btp352 (2009).

7 Anders, S., Pyl, P. T. & Huber, W. HTSeq--a Python framework to work with high-throughput sequencing data. *Bioinformatics (Oxford, England)* **31**, 166-169, doi:10.1093/bioinformatics/btu638 (2015).

8 Love, M. I., Huber, W. & Anders, S. Moderated estimation of fold change and dispersion for RNA-seq data with DESeq2. *Genome biology* **15**, 550, doi:10.1186/s13059-014-0550-8 (2014).

9 Rada-Iglesias, A. *et al.* A unique chromatin signature uncovers early developmental enhancers in humans. *Nature* **470**, 279-283, doi:10.1038/nature09692 (2011).

10 Chen, X. *et al.* Joint single-cell DNA accessibility and protein epitope profiling reveals environmental regulation of epigenomic heterogeneity. *Nature communications* **9**, 4590, doi:10.1038/s41467-018-07115-y (2018).

11 Buenrostro, J. D., Wu, B., Chang, H. Y. & Greenleaf, W. J. ATAC-seq: A Method for Assaying Chromatin Accessibility Genome-Wide. *Current protocols in molecular biology* **109**, 21.29.21-29, doi:10.1002/0471142727.mb2129s109 (2015).

12 An integrated encyclopedia of DNA elements in the human genome. *Nature* **489**, 57-74, doi:10.1038/nature11247 (2012).

13 Davis, C. A. *et al.* The Encyclopedia of DNA elements (ENCODE): data portal update. *Nucleic acids research* **46**, D794-d801, doi:10.1093/nar/gkx1081 (2018).

14 de Hoon, M. J., Imoto, S., Nolan, J. & Miyano, S. Open source clustering software. *Bioinformatics (Oxford, England)* **20**, 1453-1454, doi:10.1093/bioinformatics/bth078 (2004).

15 Saldanha, A. J. Java Treeview--extensible visualization of microarray data. *Bioinformatics (Oxford, England)* **20**, 3246-3248, doi:10.1093/bioinformatics/bth349 (2004).

16 Huang da, W., Sherman, B. T. & Lempicki, R. A. Systematic and integrative analysis of large gene lists using DAVID bioinformatics resources. *Nature protocols* **4**, 44-57, doi:10.1038/nprot.2008.211 (2009).
17 Liao, Y., Smyth, G. K. & Shi, W. featureCounts: an efficient general purpose program for assigning sequence reads to genomic features. *Bioinformatics (Oxford, England)* **30**, 923-930, doi:10.1093/bioinformatics/btt656 (2014).
18 Ramirez, F. *et al.* deepTools2: a next generation web server for deep-sequencing data analysis. *Nucleic acids research* **44**, W160-165, doi:10.1093/nar/gkw257 (2016).
19 Wallace, W. & Bear, M. F. A morphological correlate of synaptic scaling in visual cortex. *The Journal of neuroscience : the official journal of the Society for Neuroscience* **24**, 6928-6938, doi:10.1523/jneurosci.1110-04.2004 (2004).
20 McQuin, C. *et al.* CellProfiler 3.0: Next-generation image processing for biology. *PLoS biology* **16**, e2005970, doi:10.1371/journal.pbio.2005970 (2018).
21 Maximov, A. & Sudhof, T. C. Autonomous function of synaptotagmin 1 in triggering synchronous release independent of asynchronous release. *Neuron* **48**, 547-554, doi:10.1016/j.neuron.2005.09.006 (2005).

Main Figures

Figure 1 | Conditional CHD8 knockout shows CHD8 regulates ASD genes.

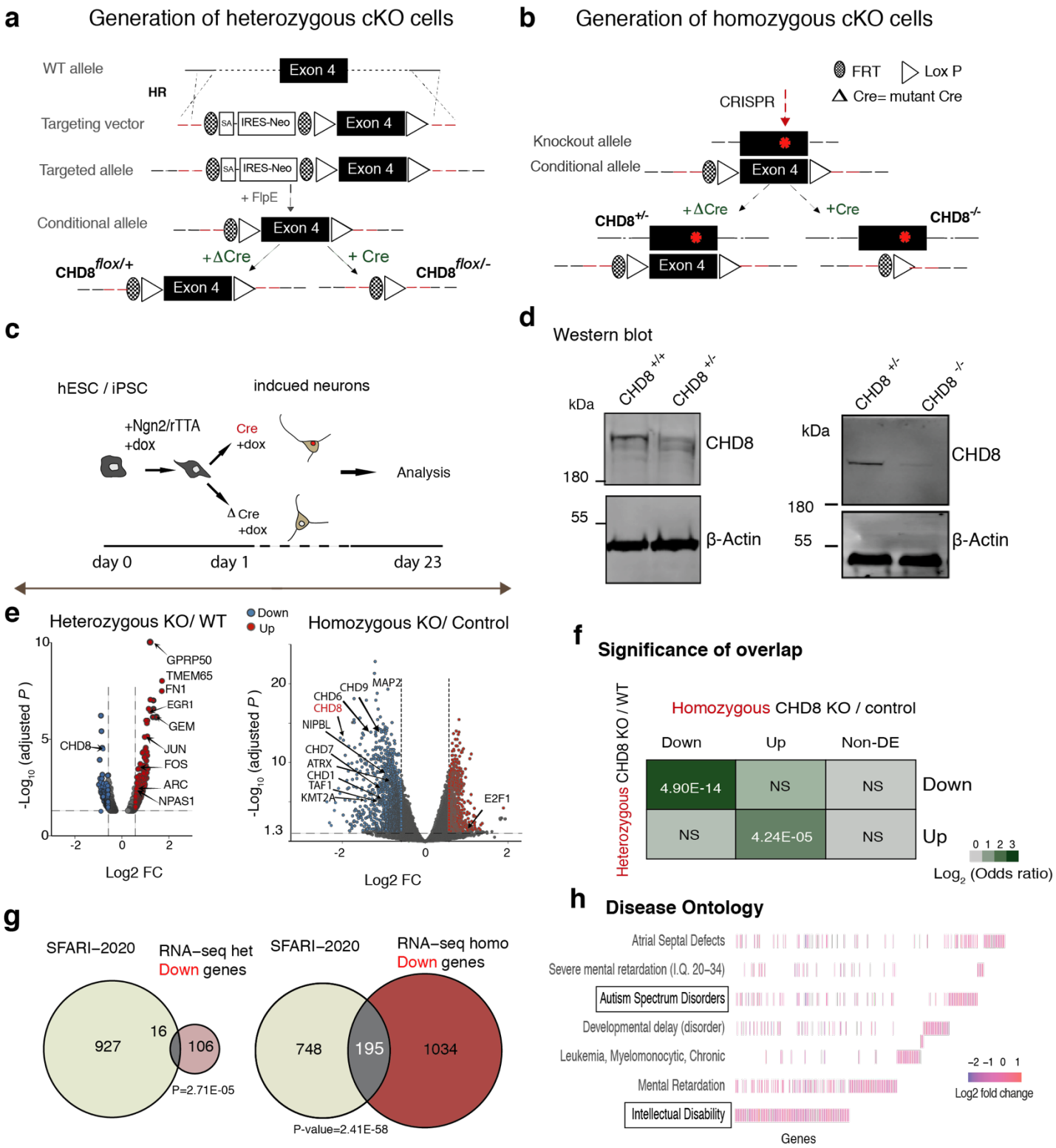

Figure 2 | Activating bindings of CHD8 enriched at ELK1 motif sites and at promoters of ASD genes.

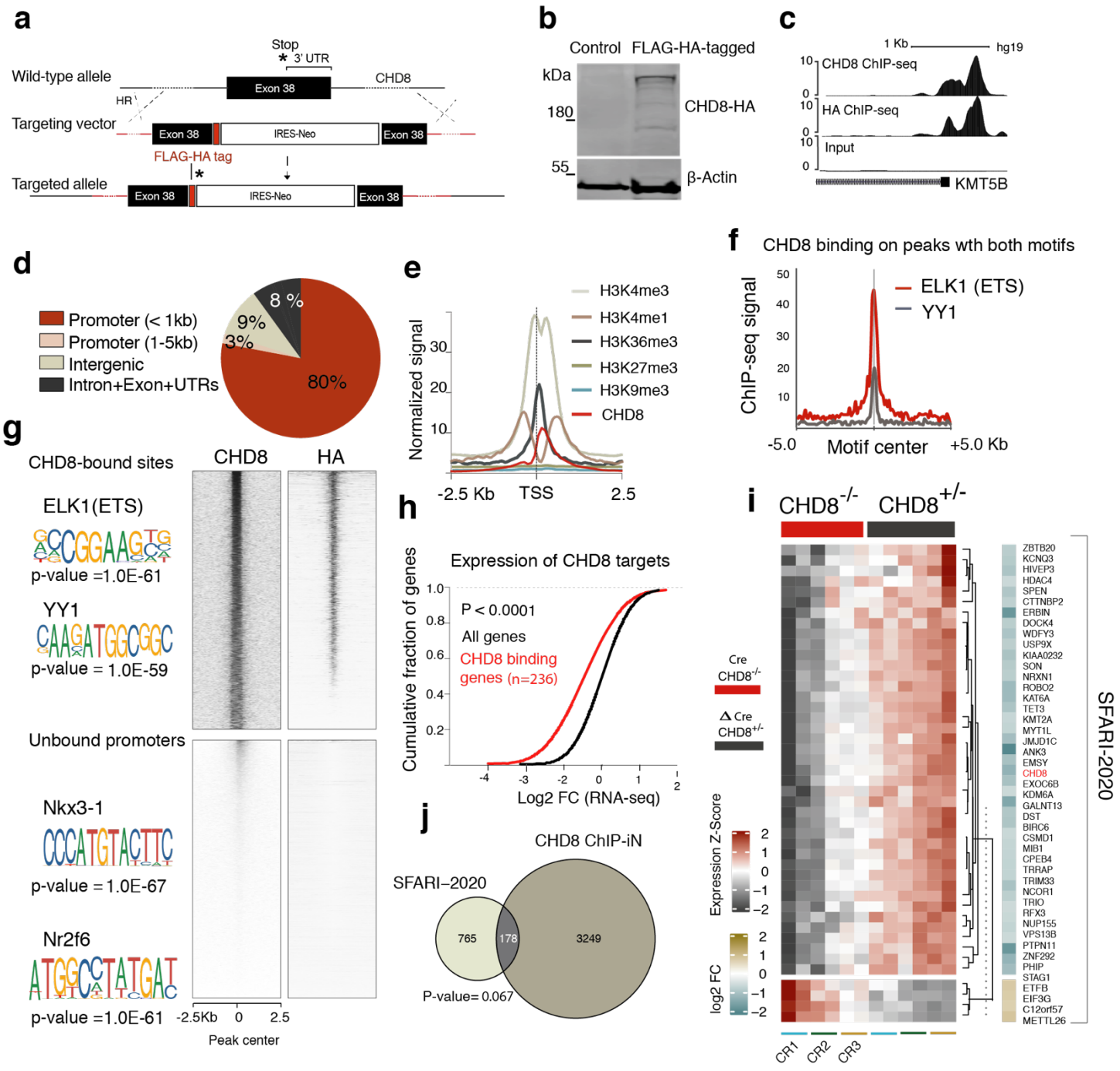

Figure 3 | Activating functions of CHD8, oriented along with the ETS motif.

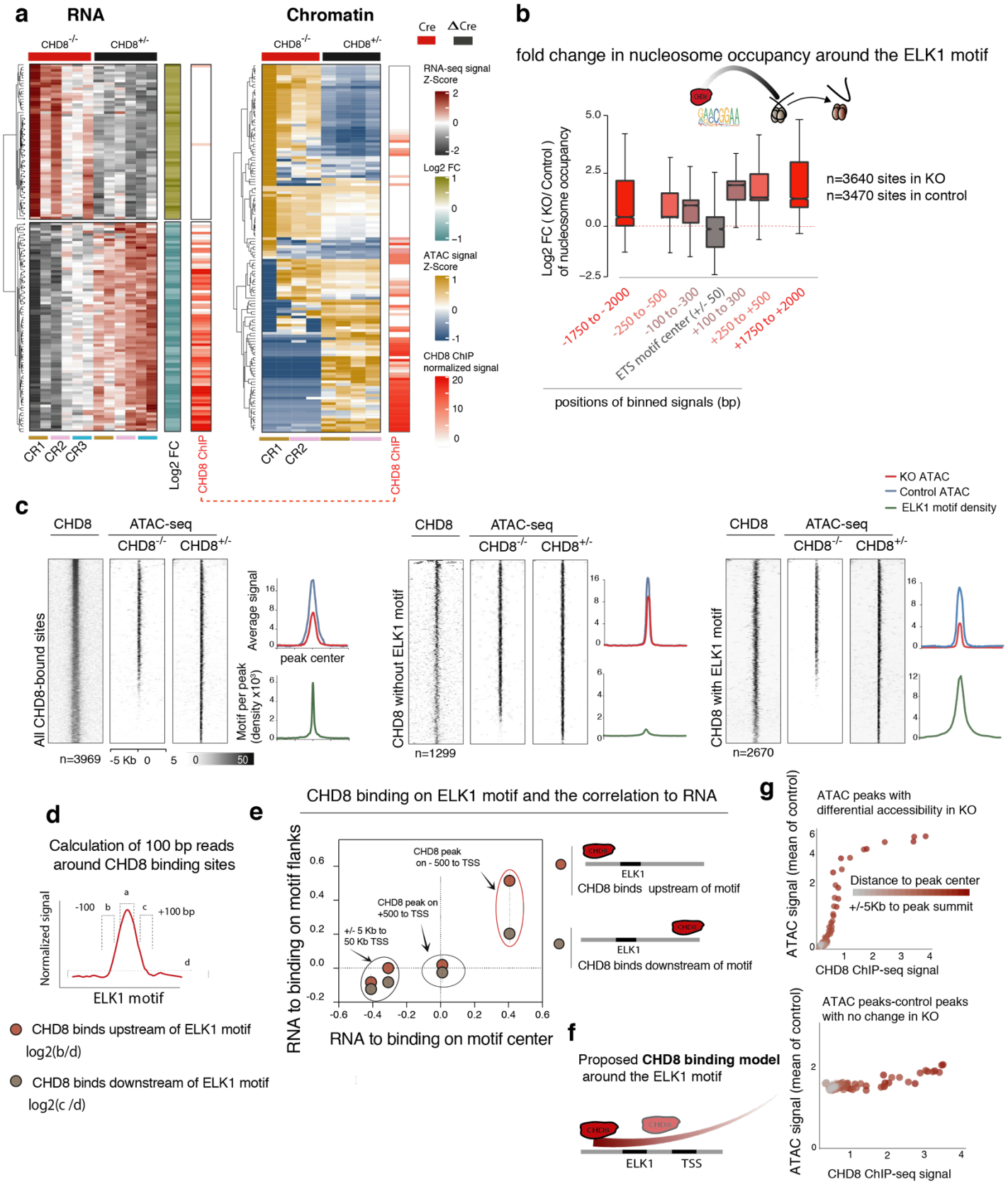

Figure 4 | Characterization of chromatin state at CHD8 targets in neurons.

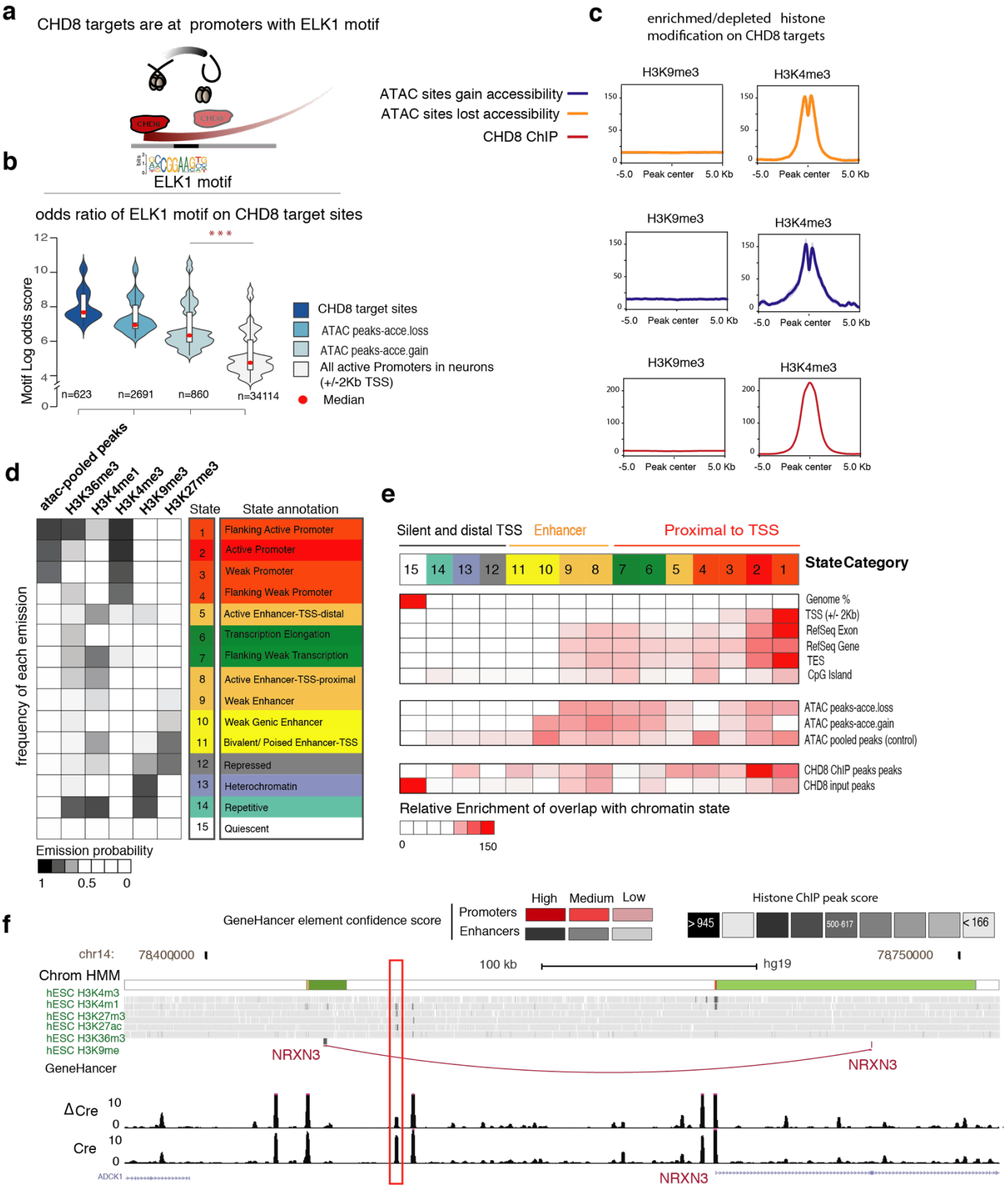

Figure 5 | CHD8 and ELK1 cooperate for chromatin targeting of CHD8 and nuclear ELK1 binding.

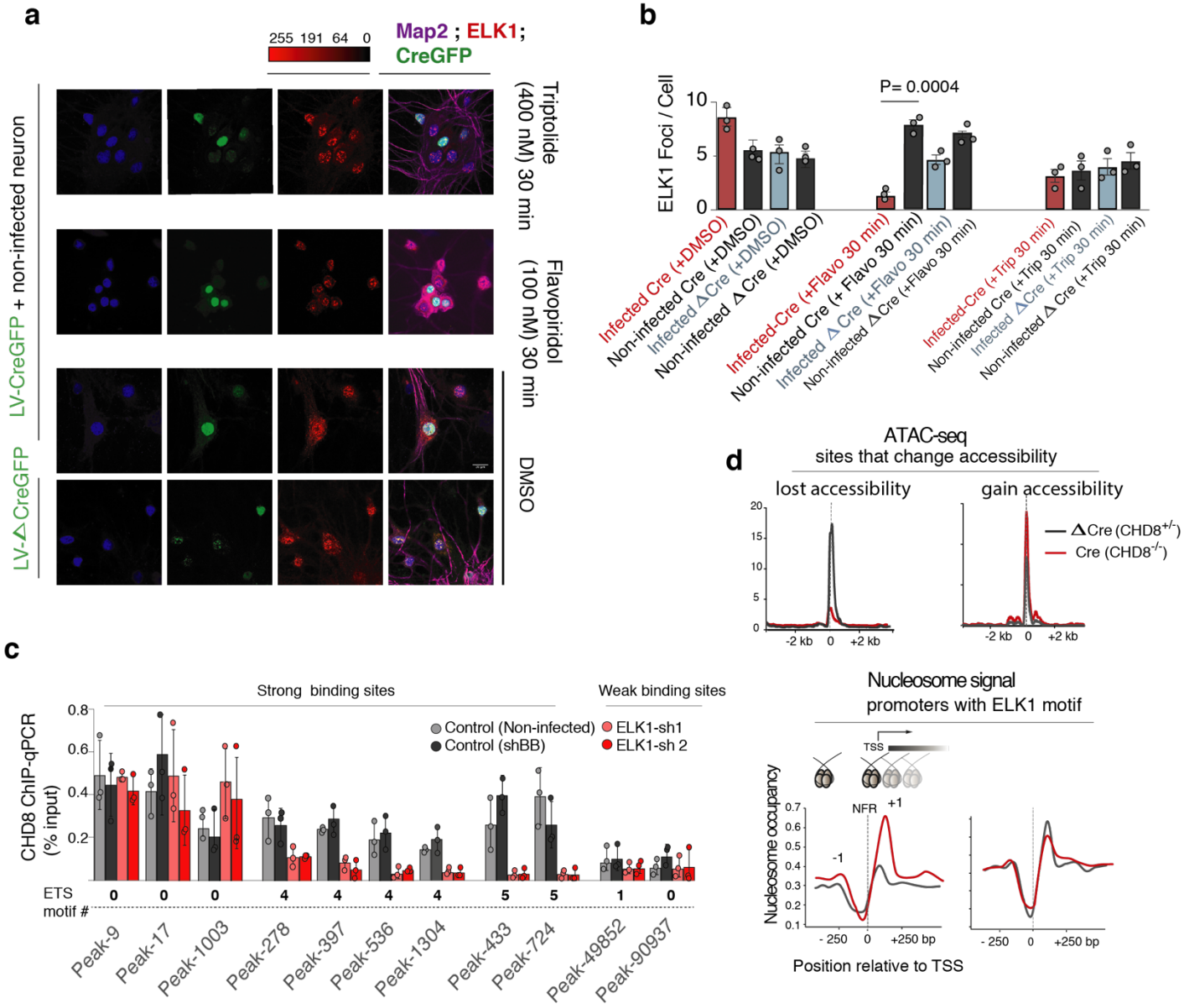

Main Figure Legends:

Figure 1 | Conditional CHD8 knockout shows CHD8 regulates ASD genes. a, Strategy to generate a heterozygous conditional knock-out (cKO) allele of *CHD8* in pluripotent stem cells (see also Extended Data Figure 1a, d). Exon 4 was flanked with LoxP sites by AAV-mediated homologous recombination. Following correct targeting, the selection cassette was removed by transient transfection with FlipE recombinase to generate the final conditional allele. Infection with Cre recombinase leads to deletion of the floxed allele and generates the mutant cells. Infection with ΔCre (inactive form of Cre) is used throughout the study to generate control cells. We obtained two correctly targeted ES and one iPS cell line (see also Extended Data Fig. 1b,c).
b, We generated homozygous *CHD8* cKO cells by introducing a CRISPR transfection-mediated indel mutation into the non-conditional *CHD8* allele causing a frameshift and early termination mutation. Infection of correctly targeted lines with Cre recombinase generates homozygous CHD8 null cells, whereas control infection with ΔCre leaves the engineered mutations unchanged. We obtained two independently mutated ES cell and one iPS cell lines (see also Extended Data Fig. 2a, b, e). **c,** Schematics of differentiation assay and conditional deletion of CHD8 at day one of differentiating human ES cells to neurons**. d** Western blot from conditional heterozygous (left) and homozygous (right) KO neurons show a decrease and a near-complete depletion of the protein in each system, respectively (the faint band is likely due to few non-infected cells)**. e,** Volcano plot of RNA-seq results in heterozygous KO and WT neurons shows modest changes in gene expression (e-left). Volcano plot of RNA-seq fold changes (FC) for differentially expressed genes (DEGs) from homozygous CHD8 KO (Cre-infected) vs. control (ΔCre -infected) neuron (e-right). **f,** Analysis for overlapping DEGs between the heterozygous and homozygous knockout RNA-seq experiment shows that the odds ratio of downregulated genes is significantly higher than overlapping upregulated genes. **g.h,** Overlap between the DEGs and ASD risk genes, obtained from SFARI-2020 list (only the downregulated genes are shown since the overlapping between the upregulated DEGs and ASD is not significant) (**g**)(1). Disease Ontology (DO) and enrichment analysis for DEGs from homozygous RNA-seq experiment show fold changes of each gene (a column is one gene) and the significance adjusted for multiple hypothesis testing and only the significantly enriched associated disease with the given DEG is plotted (**h**) (see also Extended Data Fig. 7d for implementation of Gene Set Enrichment Analysis (GSEA) to the same DEG list) (2).

Figure 2 | Activating bindings of CHD8 enriched at ELK1 motif sites and at promoters of ASD genes. a, Targeting strategy to insert a C-terminal FLAG-HA tag at the endogenous *CHD8* locus (see also Extended Data Fig. 4a-d). **b,** Western blot analysis of tagged and non-tagged (control) ES cells

using HA antibodies shows a band at the expected size of CHD8 corresponding to endogenous CHD8. **c**, An example of a CHD8 peak at the promoter of the *KMT5B* locus. **d,** CHD8 binds primarily at proximal promoter regions. Pie chart shows the distribution of CHD8 ChIP-seq peaks across the genomic regions in ES cell-derived neurons. Top heatmaps are bindings of CHD8 shown as overlapping peaks between two ChIP-seq experiments, taken from two separate pull-down with HA and CHD8 antibody (MACS2 adjusted $p < 0.05$, n=3696 peaks overlapping peaks). Using HOMER and MEME, we found that ETS and YY1 motifs enriched at CHD8-bound sites (see also Extended Data Fig. 5d, f, also Extended Data Fig 6a). The bottom heatmap is the same ChIP-seq signals, stratified on CHD8-unbound promoters (n=4000). The greyscale shows the normalized coverage for all groups (3, 4). **e**, CHD8 binding sites are enriched at genomic sites showing an enrichment of active histone modifications (taken from ENCODE data for H9 cell-derived neurons) (see also Extended Fig. 5b,e) (5). **f**, The normalized signal of CHD8 on peaks with both YY1 and ELK1(ETS). **h**, Expression of genes with significant CHC8 peak on the promoter (+/- 5Kb) shows a marked decrease, compared to control. **i,** Gene expression of ASD genes with CHD8 binding at promoters and also with significant expression change in RNA-seq experiment. **j**, Overlapping of SFARI gene list and CHD8 bound genes. Significance calculated with hypergeometric distribution.

Figure 3 | Activating functions of CHD8, oriented along with the ETS motif. a, Heatmaps show RNA expression (left) and the promoter accessibility (right) of **136** genes with a significant change in KO. Normalized CHD8 binding signal plotted at the side of each heatmap and sorted with the same order of the respective heatmap. **b,** Fold change of nucleosome occupancy around the ELK1 motif, across the genome, and in the binned regions. In *CHD8*-KO, nucleosome density increases, but not at the center of the ELK1 motif, rather it is away from the ELK1 motif in the 3` direction. **c**, Normalized CHD8 signal and ATAC-seq signal in *CHD8*-KO and the control samples plotted as a heatmap, and ELK1 motif density plotted as a green enrichment plot. Genome-wide ChIP-seq and ATAC-seq signal divided into three groups: sites with exclusive enrichment for ELK1 motif, sites without ELK1 motif, and the control sites, which are the randomly shuffled peak sets. For each group, compare the ATAC signal from KO to the control sample. **d**, Illustration shows sample enrichment plot for CHD8 binding signal and the calculations of CHD8 binding at sites indicated (+- 100bp, around the CHD8 peak). CHD8 binding signal at ELK1 motif occurs either upstream or downstream of CHD8 peak summit. Therefore, CHD8 binding signal taken from 100 bp at each site and normalized to the background signal, which is the average signal at “d” region. **e**, Correlation of RNA (average FPKM) to CHD8 binding signal. RNA is the expression of the closest gene to CHD8 peak. CHD8 binding is divided into six regions with respect to ELK1 motif directionally and the TSS (+500 bp TSS, -500 TSS, +-5Kb to 50Kb TSS, and see the Schematic in "e-right" for classification of ELK1 motif around the CHD8

peaks). **g**, Enrichment of ChIP-seq signal (CHD8 binding) and ATAC signal (average ATAC signal in control samples) on sites with differential accessibility in *CHD8* KO neurons. CHD8 binding enriches on sites with a significant change in differential accessibility (ATAC detected), compared to sites with no change.

Figure 4 | Characterization of chromatin state at CHD8 targets in neurons. a,b, Log odds ratio of ELK1 motif shows ELK1 motif enrichment. There is a marked increase of ELK1 motif at direct binding sites of CHD8 and regions of ATAC that lost accessibility. **c**, Enhancement of distinct histone modification at CHD8 binding and ATAC-seq sites shows patterns of activating (H3K4me3) and repressive (H3K9me3) modification. **d**, ChromHMM analysis of chromatin modification enrichment and the annotation of the genomic feature with transition probability for a 15-state model. **e**, Distribution, and relative enrichment of CHD8 binding and the ATAC sites across all chromatin states in neurons. **f**, Example of a chromatin state model signal track along with histone modification ChIP signal track in neurons. The GeneHancer track is loaded to reveal predicted candidate promoters and enhancers (see also Extended Data Figure 10. a, that shows fold enrichment of annotated chromatin state annotated TSS).

Figure 5 | CHD8 and ELK1 cooperate for chromatin targeting of CHD8 and nuclear ELK1 binding. a, b, Representative immunofluorescence images of neurons treated for 30 minutes with transcription inhibitors (Flavopiridol and Triptolide) or DMSO. Within each coverslip, the number of ELK1 foci (or puncta) from one GFP positive (lentivirus CreGFP, or ΔCreGFP infected), in the nuclear area compared to a non-infected cell at the proximity, to avoid potential artifacts. ROIs are defined in the DAPI channel. The scale bar is 20 um. **c**, ChIP-qPCR analysis for CHD8 binding at selected peaks, when ELK1 is KD or with control shRNA. The number of ETS motif at each peak site is written beneath the peaks. There was no change in CHD8 binding at sites without ETS motif. See also Extended Data Fig. 11a,b for validation of CHD8 binding on the peaks in CHD8-KO neurons, and also Extended Data Fig. 11c for validation of the short hairpin knockdown and also Extended Data Fig. 11d for validation of ELK1 motif specificity to CHD8 binding using control ETS factor knockdown. **d**, The top plot is the normalized ATAC-seq signal in *CHD8*-KO and control, on sites that change accessibility. The bottom plot is the normalized cross-correlation of ATAC-seq signal, to measure nucleosome density analysis. The enrichment plot is a subset of the calculated nucleosome density signal, only at the promoters with ELK1 (ETS) motif.

Extended Figures

Extended Data Figure 1. | Targeting the *CHD8* gene in human pluripotent stem cells.

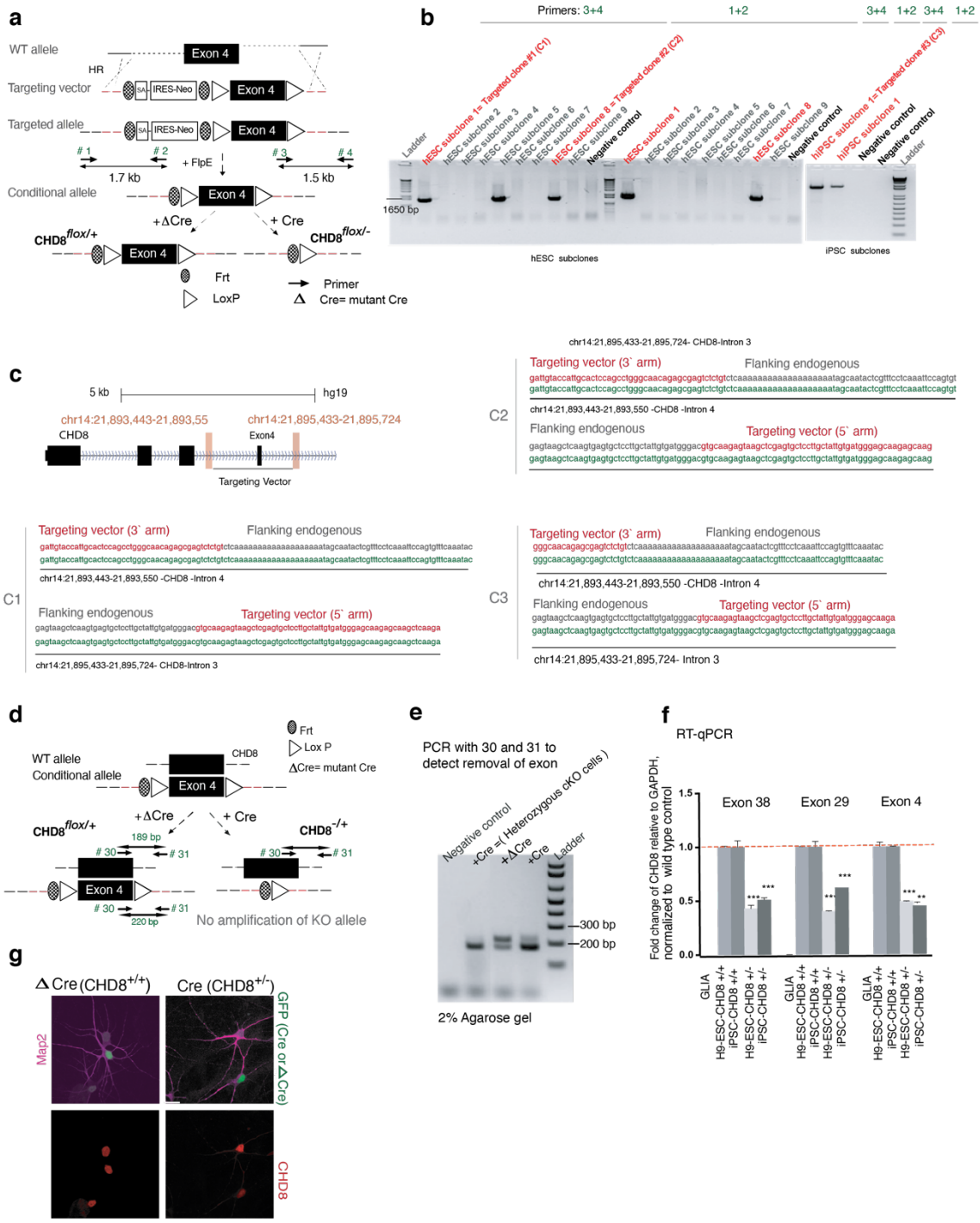

Extended Data Figure 2 | Characterization of conditional homozygous *CHD8* knockout neurons.

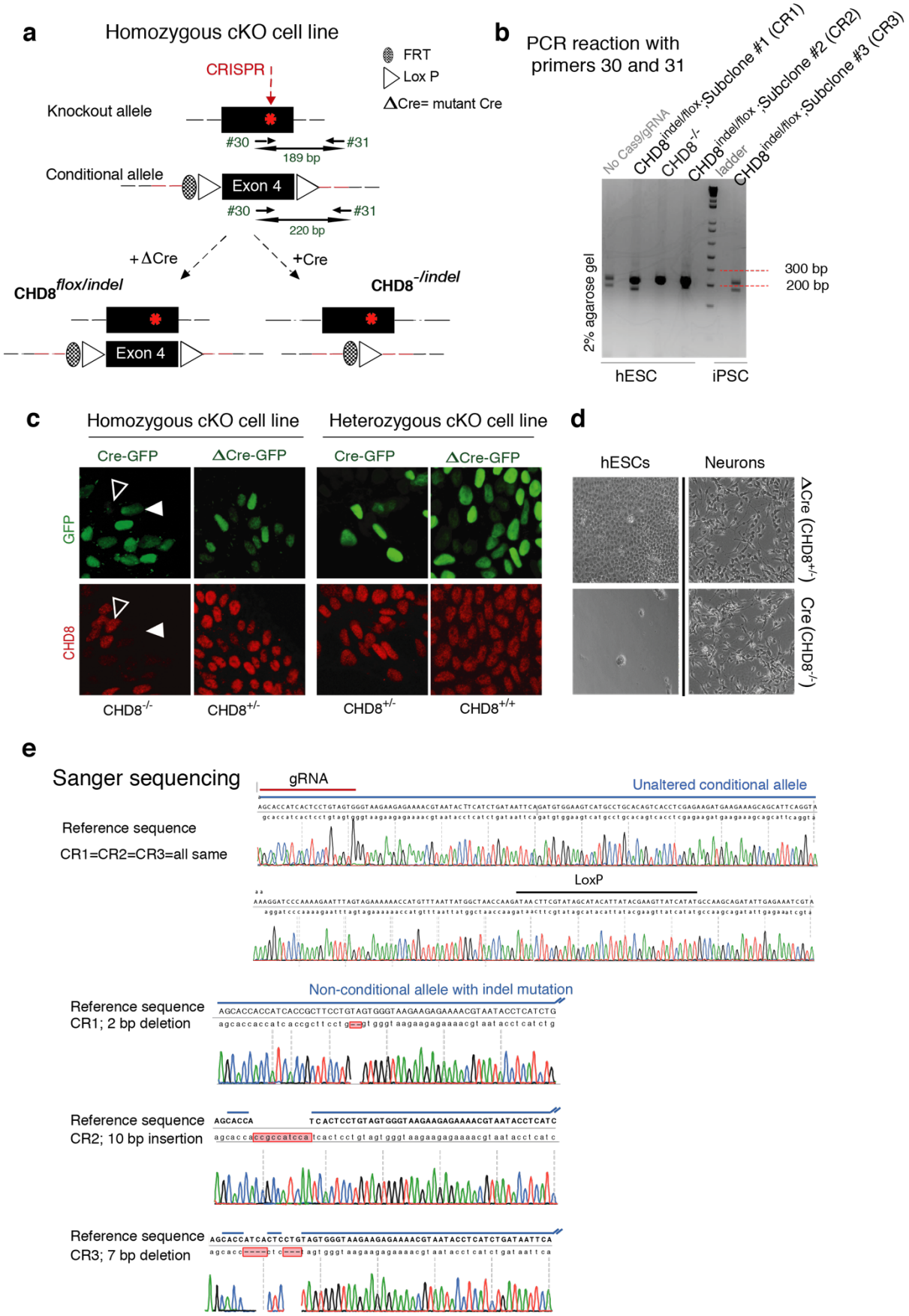

Extended Data Figure 3 | Electrophysiological characterization of heterozygous and homozygous *CHD8* KO neurons.

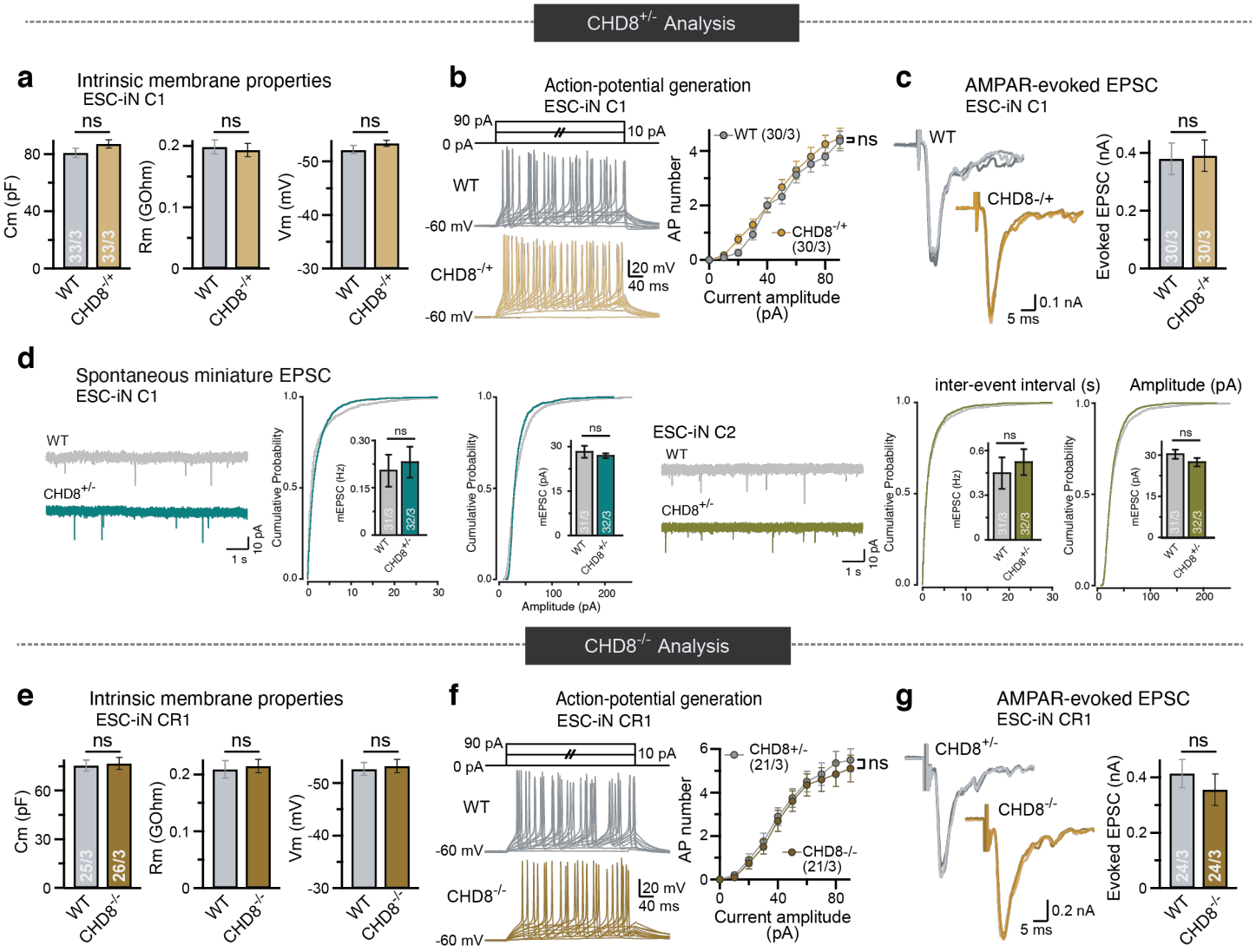

Extended Data Figure 4 | Insertion of an epitope tag into the C-terminus of the *CHD8* gene.

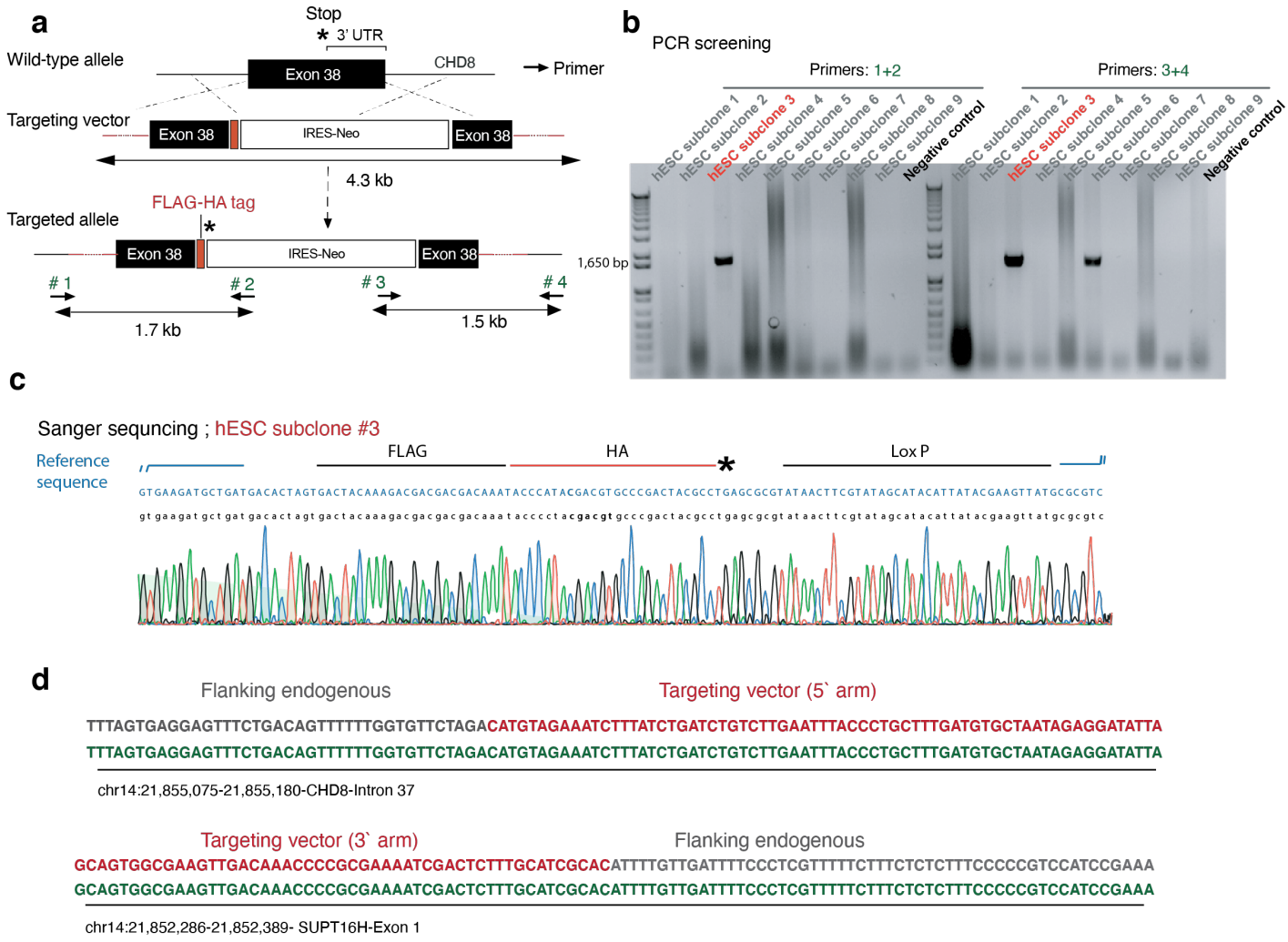

Extended Data Figure 5 | Activating CHD8 bindings are at promoters.

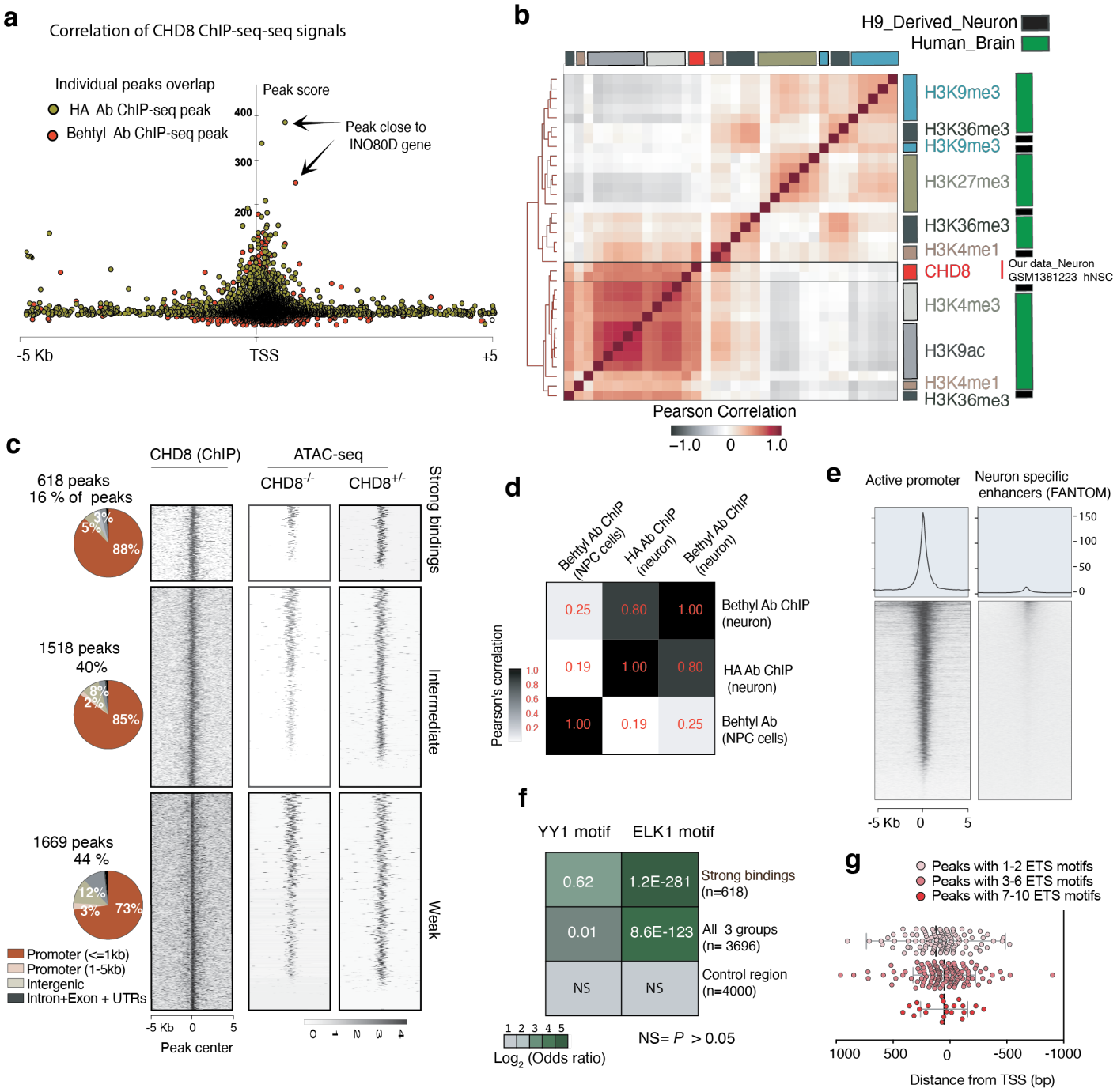

Extended Data Figure 6 | ETS motif enrichment is specific for CHD8-bound promoters.

a

Top motifs on all CHD8 binding sites and the promoters of affected genes in CHD8-KO neurons (ATAC-seq experiment)

Experiment	Best match motif	p-value	Motif logo (forward strand)	Alignment to the consensus	Match score (0-1)	% of peaks with motif	% of background sequences with motif	Fold enrichment	Rank
ChIP-seq	Elk1(ETS)	1.0E-61		RCCGGAAGYG RCCGGAAGTD	0.97	71.14%	32.82%	2.2	1
	YY1	1.0E-59		CAASATGGCGGC CAAGATGGCGGC	0.98	24.64%	12.20%	2.0	2
ATAC-seq (Closig sites)	POL004.1	1.0E-28		--CRRCCAATCA ACTAGCCAATCA	0.93	13.30%	5.63%	2.3	1
	ELF1(ETS)	1.0E-27		--CCGGAAGT ANCCGGAAGT	0.98	19.04%	9.57%	2	2

b

Top 30 motifs on all active promoters with CHD8 binding

Motif Name	p-value	Match score (0-1)	% of peaks with motif	% of background sequences with motif	Fold enrichment	Rank
Elk1(ETS)	1.00E-61	0.97	18.7%	8.3%	2.24	1
YY1	1.00E-59	0.98	43.4%	28.4%	1.53	2
Elk4(ETS)	1.00E-48	0.82	61.6%	46.4%	1.33	3
ELF1(ETS)	1.00E-48	0.63	62.6%	47.4%	1.32	4
Fli1(ETS)	1.00E-41	0.62	56.5%	42.5%	1.33	5
GABPA(ETS)	1.00E-35	0.71	70.2%	57.6%	1.22	6
ETV4(ETS)	1.00E-31	0.85	59.0%	46.8%	1.26	7
Eif4(ETS)	1.00E-31	0.85	71.5%	59.9%	1.19	8
ETV1(ETS)	1.00E-22	0.67	55.3%	45.2%	1.22	9
ETS1(ETS)	1.00E-21	0.72	68.0%	58.2%	1.17	10
ZFX(Zf)	1.00E-19	0.71	56.9%	47.5%	1.20	11
ZNF711(Zf)	1.00E-18	0.63	66.0%	57.1%	1.16	12
GFY	1.00E-16	0.51	85.6%	78.9%	1.08	13
EWS:FLI1-(ETS)	1.00E-13	0.61	12.1%	7.5%	1.61	14
Ronin(THAP)	1.00E-13	0.62	34.9%	27.8%	1.26	15
Etv2(ETS)	1.00E-12	0.71	10.9%	6.8%	1.60	16
ELF5(ETS)	1.00E-10	0.66	46.2%	39.4%	1.17	17
ERG(ETS)	1.00E-10	0.74	11.5%	7.6%	1.51	18
EHF(ETS)	1.00E-10	0.63	35.3%	29.2%	1.21	19
ZNF143|STAF(Zf)	1.00E-08	0.67	63.1%	57.3%	1.10	20
NRF1(NRF)	1.00E-07	0.81	51.4%	45.7%	1.12	21
ETS:RUNX	1.00E-07	0.76	19.5%	15.5%	1.26	22
NRF(NRF)	1.00E-06	0.76	28.3%	23.8%	1.19	23
E2F4(E2F)	1.00E-06	0.71	7.9%	5.4%	1.47	24
SPDEF(ETS)	1.00E-04	0.61	26.5%	22.8%	1.16	25
PU.1-IRF(ETS:IRF)	1.00E-04	0.71	54.9%	50.6%	1.09	26
CRE(bZIP)	1.00E-04	0.57	42.0%	37.8%	1.11	27
Rfx2(HTH)	1.00E-04	0.71	44.4%	40.3%	1.10	28
ELF3(ETS)	1.00E-04	0.71	18.9%	15.9%	1.19	29
Zac1(Zf)	1.00E-03	0.65	8.2%	6.3%	1.31	30

c

Top 30 motifs on all active promoters with exclusion of CHD8-bound promoters

Motif Name	p-value	Match score (0-1)	% of peaks with motif	% of background sequences with motif	Fold enrichment	Rank
Nkx3-1	1.00E-67	0.61	1.98%	0.34%	5.82	1
Nr2f6	1.00E-61	0.66	1.50%	0.19%	7.89	2
ZBTB18	1.00E-27	0.69	1.68%	0.60%	2.80	3
TBP	1.00E-25	0.86	9.07%	6.40%	1.42	4
ZNF143	1.00E-23	0.67	0.54%	0.06%	9.00	5
TWIST1	1.00E-21	0.60	2.34%	1.17%	2.00	6
Foxa2	1.00E-20	0.63	12.31%	9.55%	1.29	7
LIN54	1.00E-19	0.61	24.94%	21.22%	1.18	8
Foxj1	1.00E-19	0.60	8.05%	5.83%	1.38	9
Brn2	1.00E-19	0.84	9.04%	6.71%	1.35	10
Pou6f1_2	1.00E-18	0.69	17.14%	14.05%	1.22	11
NR1A4	1.00E-18	0.72	5.47%	3.73%	1.47	12
ZEB1	1.00E-17	0.70	0.41%	0.05%	8.20	13
CTCFL	1.00E-17	0.66	3.00%	1.76%	1.70	14
Tcf3	1.00E-17	0.63	4.54%	3.00%	1.51	15
Foxd3	1.00E-17	0.61	11.65%	9.17%	1.27	16
Hand2	1.00E-16	0.60	3.08%	1.85%	1.66	17
RUNX1	1.00E-16	0.64	0.38%	0.05%	7.60	18
Esrra	1.00E-15	0.68	0.68%	0.19%	3.58	19
Gata1	1.00E-15	0.64	3.50%	2.21%	1.58	20
Klf4	1.00E-15	0.64	3.06%	1.85%	1.65	21
XCPE1	1.00E-15	0.66	1.57%	0.75%	2.09	22
Egr1	1.00E-14	0.66	1.93%	1.03%	1.87	23
RUNX1	1.00E-14	0.68	9.03%	7.01%	1.29	24
ZIC1	1.00E-14	0.74	0.54%	0.13%	4.15	25
RUNX2	1.00E-13	0.64	10.03%	7.99%	1.26	26
Irx5	1.00E-12	0.60	34.68%	31.47%	1.10	27
Smad3	1.00E-12	0.65	0.65%	0.22%	2.95	28
CEBPA	1.00E-11	0.68	0.93%	0.40%	2.33	29
CUX2	1.00E-11	0.71	4.28%	3.04%	1.41	30

Extended Data Figure 7 | Relevance of CHD8 binding for transcriptional regulation, chromatin remodeling activity, and ASD gene regulation.

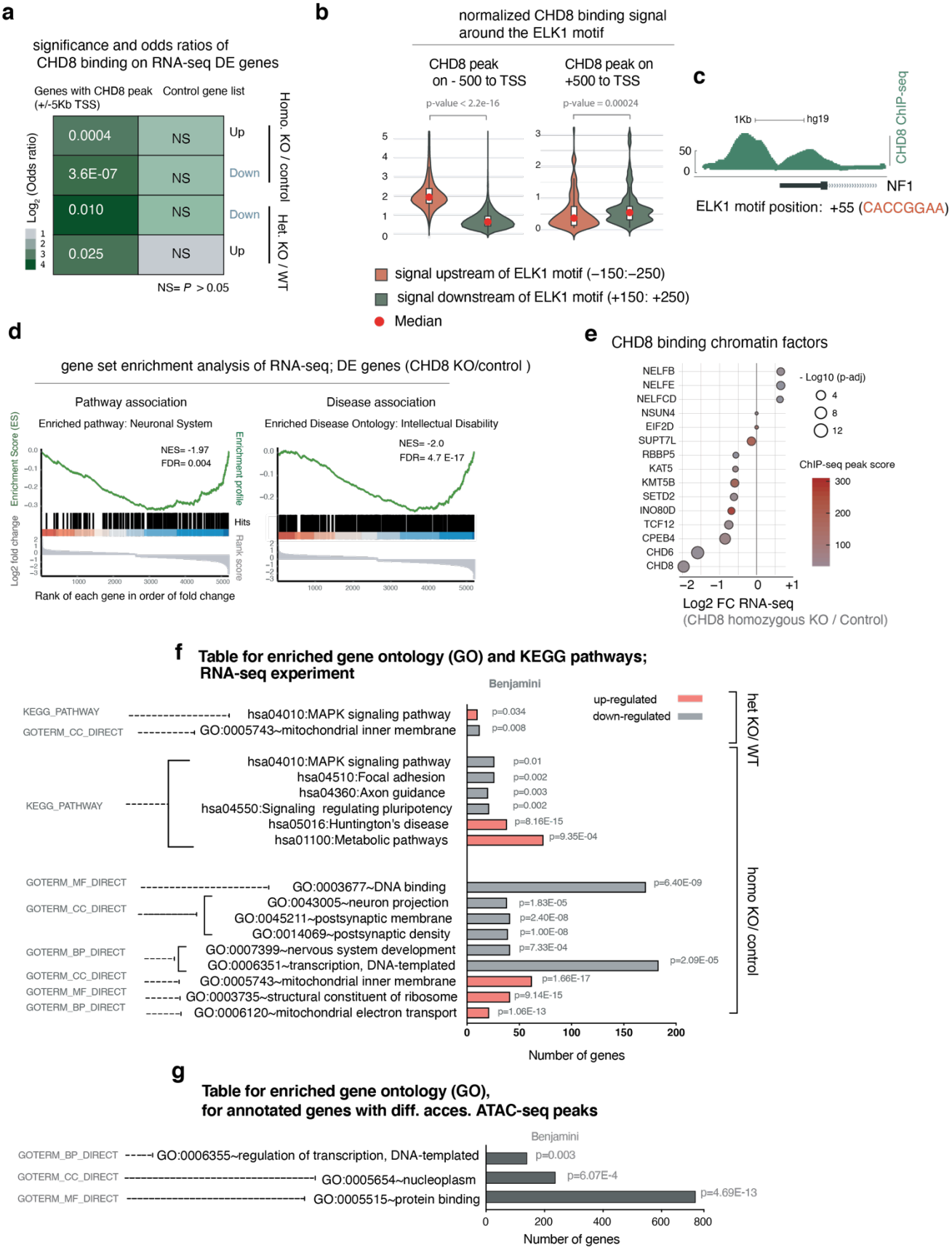

Extended Data Figure 8 | CHD8 promotes chromatin accessibility and transcriptional activation in human neurons.

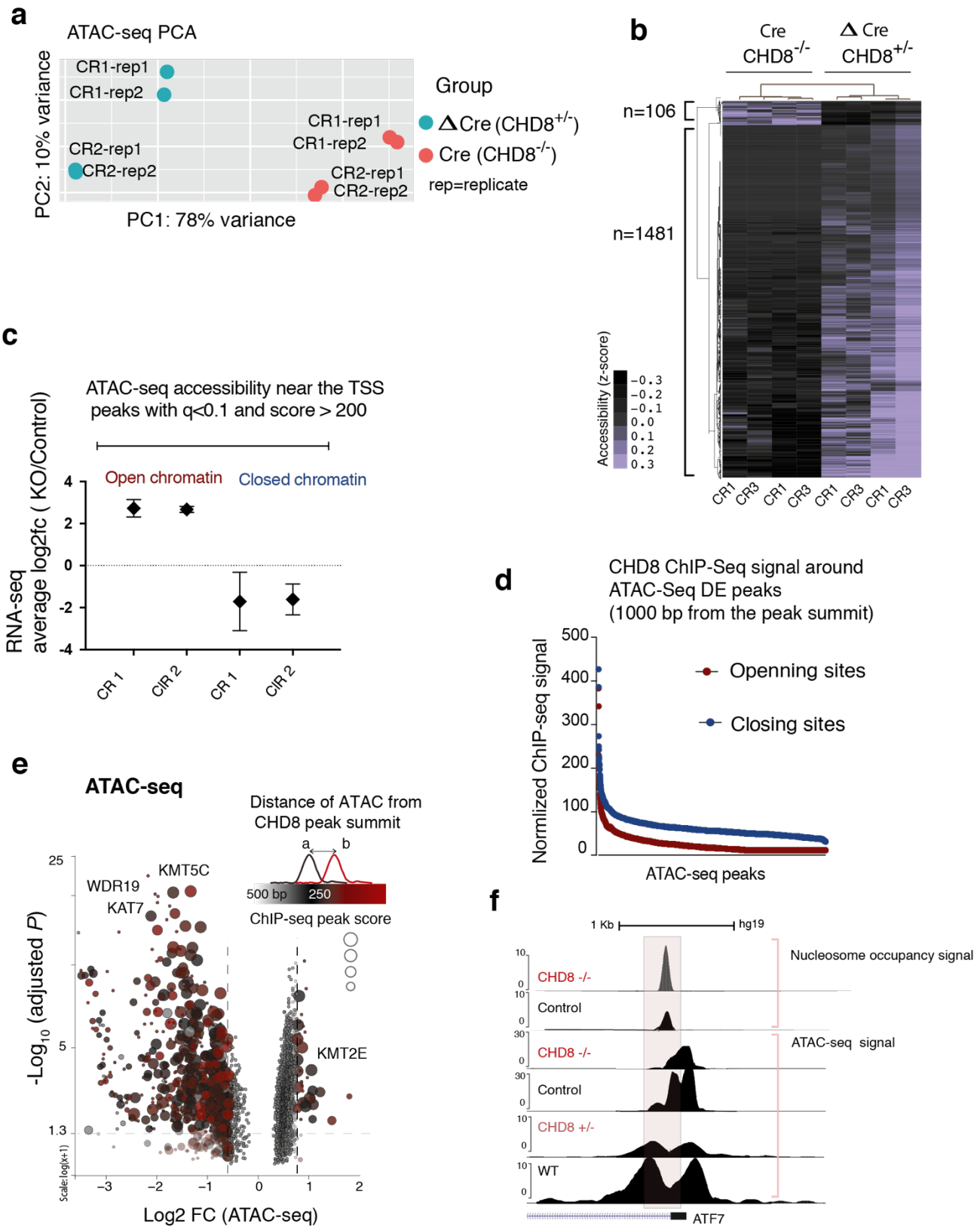

Extended Data Figure 9 | CHD8 positively regulates a group of high confident ASD genes in neurons.

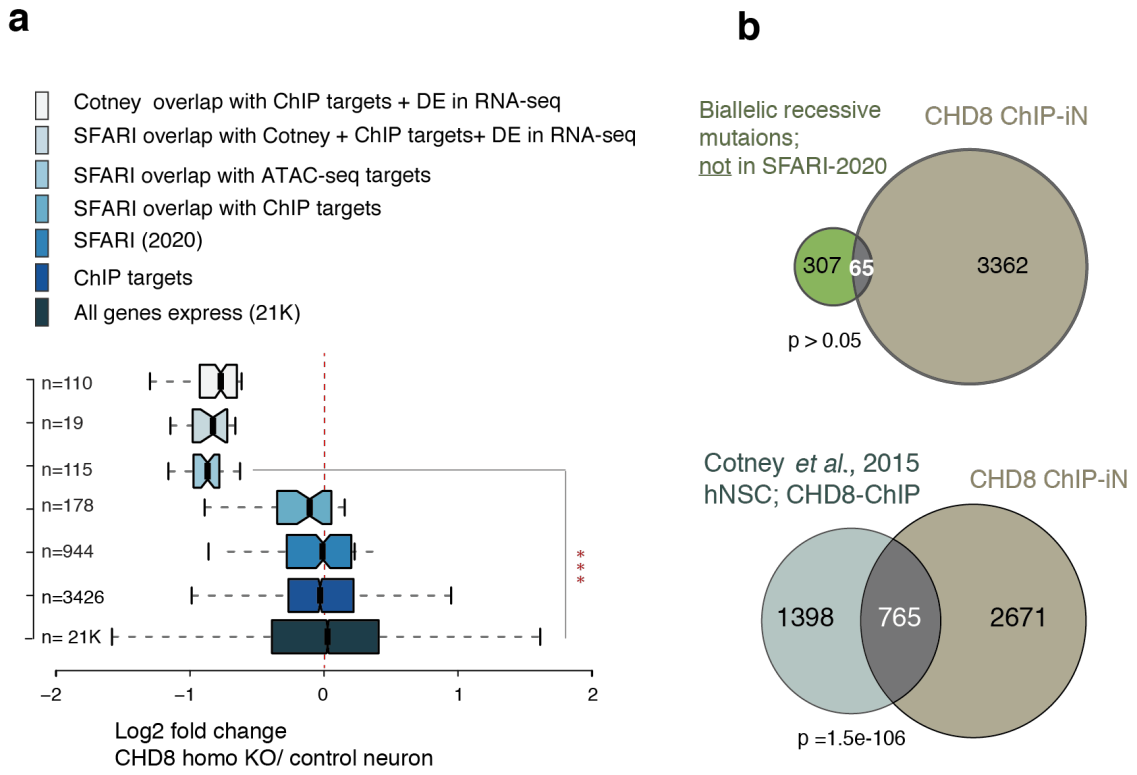

Extended Data Figure 10 | Chromatin state and target genes of CHD8 in ATAC-seq.

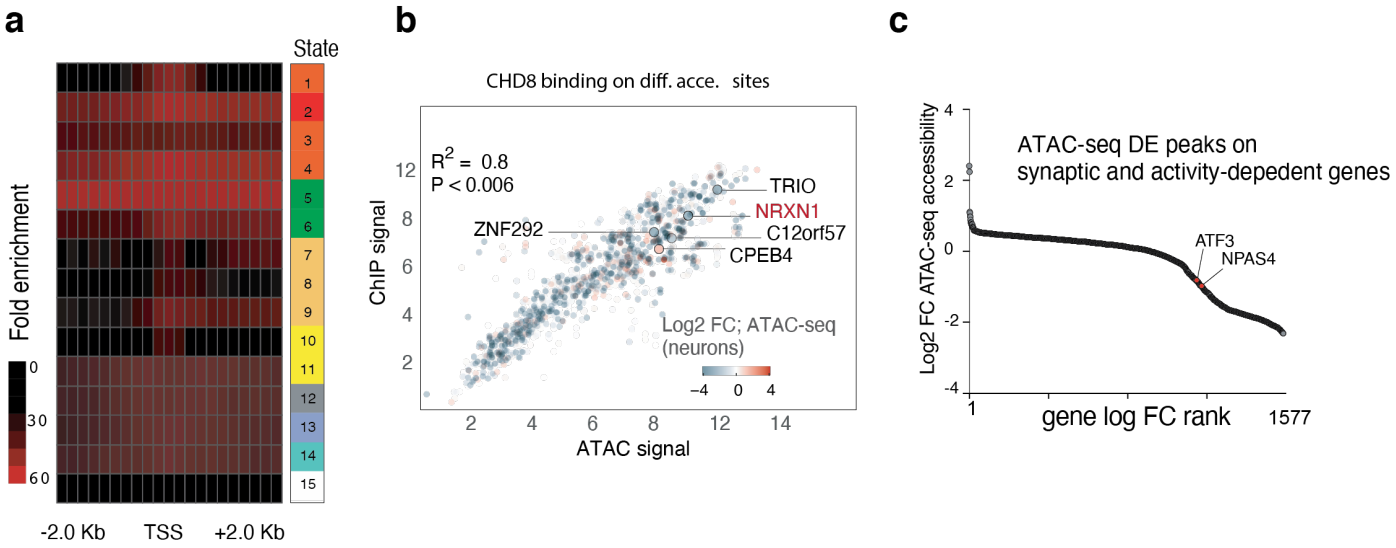

Extended Data Figure 11 | CHD8 binding to ETS-enriched promoters, functionally depends on ELK1.

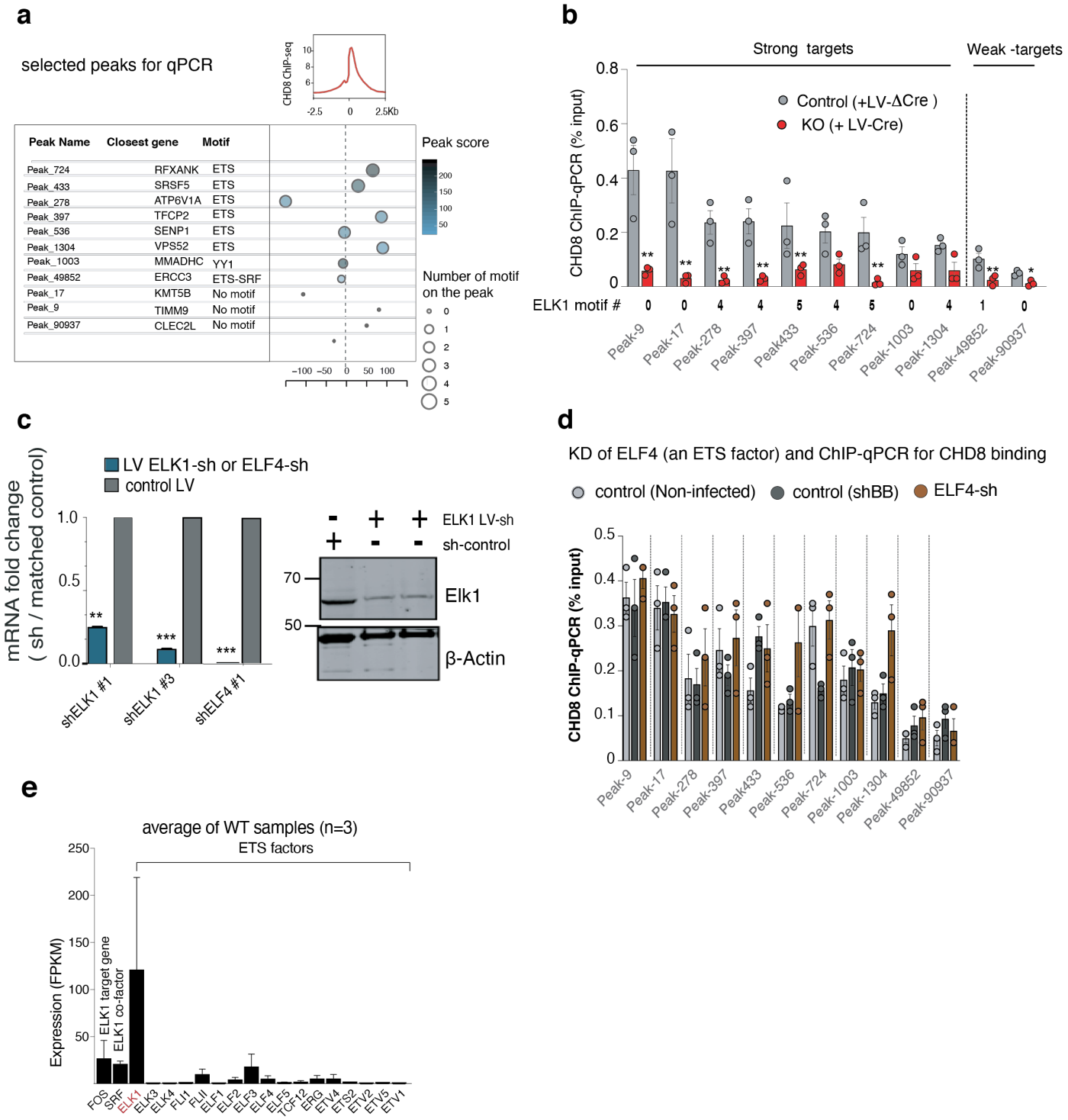

Extended Figure Legends

Extended Data Figure 1. | Targeting the *CHD8* gene in human pluripotent stem cells. a, Targeting strategy for generating a conditional KO allele of the *CHD8* gene by flanking exon 4 with LoxP sites. Deletion of exon 4 is predicted to create a frameshift mutation with early truncation. **b**, Screening PCR using external primers designed for outside the homology arm towards inside the targeting vector identified two subclones from hESC (C1 & C2) and one subclone from iPSC (C3) that were positive for the insertion of the targeting vector. **c**, Sanger sequencing is spanning the transition of the targeting arms into endogenous sequences demonstrating correct targeting of the construct into the *CHD8* locus (clones C1,C2, and C3). **d**,**e**, Excision of exon 4 after infection with LV-Cre and screening with the primers around the loxP sites (primer #30 and #31) result in a single band in heterozygous KO compared to two bands in WT cells as expected. **f,** Quantitative reverse transcription PCR (RT-qPCR) using the probes for three exons shows the levels of mRNA decreases in heterozygous KO neurons. **g**, Immunofluorescence analysis of heterozygous KO and WT neurons for Map2 and CHD8. The nuclear staining signal intensity significantly decreases in heterozygous mutant neurons.

Extended Data Figure 2 | Characterization of conditional homozygous *CHD8* knockout neurons.
a, Introduction of an indel mutation by CRISPR-CAS9 to non-conditional exon 4 of *CHD8* gene, to generate a conditional homozygous knock out cells. **b**, Validation of the genotype by PCR around the loxP sequence (spanning the gRNA targeting region) which amplifies two bands due to one allele being 32 bp smaller than the other. Therefore, the top band corresponds to the floxed allele and the bottom band to the non-conditional allele, a candidate for carrying an indel mutation. Each band is gel-purified, TOPO cloned, and sequenced using M13 forward and M13 reverse primers (CR1, CR2; both hESC, and CR3, is an iPSC subclone, confirmed to carry an indel mutation in non-floxed allele). **c**, Sanger sequencing of floxed and non-floxed alleles identified three subclones that carry frameshift indel mutations in the non-conditional allele with an un-altered floxed allele. Note that the conditional exon is shown only once as the representative sequence for all three subclones.

Extended Data Figure 3 | *Electrophysiological* characterization of heterozygous and homozygous *CHD8* KO neurons. a, E*lectrophysiological* recordings of the intrinsic membrane properties in the C1 line, a heterozygous conditional KO line: capacitance (Cm), resting membrane potential (Vm), and input resistance (Rm). N=33 recorded cells in 3 batches (see numbers in bars). Student's t-test. **b**, Active membrane properties demonstrated by step-wise current injection protocol.

The number of action potentials in response to current amplitude is plotted (right). **c**, Amplitude of evoked excitatory postsynaptic currents (EPSCs) in clone C1 showed no changes between the heterozygous KO and the WT neurons. **d**, Amplitudes and frequency of spontaneous miniature EPSC (mEPSCs) in the presence of 1μM tetrodotoxin showed no change between CHD8 heterozygous KO and WT neurons in clone C1 and clone C2, N=31 or 32, respectively in 3 batches. Student's t-test. **e**, Analysis of the conditional homozygous mutant cell line CR1. Shown are capacitance, input resistance, and resting membrane potential. **f**, Active membrane properties of CR1-derived iN cells as in b. **g**, Recording of evoked excitatory postsynaptic currents (EPSCs) CR1-derived iN cells shows no statistically significant difference between Cre and **Δ**Cre ($Chd8^{-/-}$ vs. $Chd8^{+/-}$) neurons. N=24 cells in 3 batches, Student's t-test.

Extended Data Figure 4 | Insertion of an epitope tag into the C-terminus of the *CHD8* gene. a, Schematic of targeting strategy for insertion of FLAG-HA tag to the C-terminus region of CHD8 gene in the frame. Throughout the manuscript we have used the HA tag for downstream experiments. **b,** Screening PCR of neomycin resistant hESC colonies with external primers, i.e., one primer outside of the homology arms and one primer inside the targeting vector (primer #1 and #4). **c**, Sanger sequencing to detect the correct insertion of donor vector in the C-terminus region. **d**, Sanger sequencing to validate the correct transition of targeting vector into endogenous arms (black line after the blue lines on both sides).

Extended Data Figure 5 | Activating CHD8 bindings are at promoters. a, ChIP-seq peaks from CHD8 antibody and HA antibody pull-down experiments. We observed a high degree of overlap at high confidence peaks and proximal to the transcription start site (TSS). **b**, Pearson correlation of CHD8 ChIP-seq signal (averaged for the entire genome taken from both experiments) and histone modification from H9-derived neurons. The histone mark ChIP-seq data obtained from Encyclopedia of DNA Element Elements (ENCODE) repository and the accession number is cited in "ChIP-seq-peaks.xls" file (5). **c** K-means clustering ChIP-seq signal into three groups based on peak score shows recognizes the most specific targets of CHD8 binding that are at promoters. ATAC-seq signal from homozygous KO and control on all three regions show a marked on strong binding sites of CHD8**. d,** Pearson's correlation between normalized CHD8 ChIP-seq signals from two antibody pull-down and a previously published CHD8 ChIP-seq dataset in NPC cells (GSE61492)(6).
e, Heatmap of CHD8 binding signal, at promoters of neural genes and enhancers. **f**, Quantitative assessment of motif enrichment at CHD8 binding from odds ratio calculations of motif enrichment at (1) strong CHD8 binding sites, (2) the non-specific binding sites and (3) control sites (randomly

shuffled peaks, at third row). 1 and 2 are taken from clustering analysis in Extended Data Figure 5c. **g**, ETS motifs spread closely around TSS at CHD8 peak regions.

Extended Data Figure 6 | ETS motif enrichment is specific for CHD8-bound promoters. a, DNA motif enrichment analysis showed significant enrichment of ETS motifs in CHD8-bound sites and the regions of ATAC-seq with the change in chromatin accessibility. **b,** ETS factor motif (red highlights) is over-represented in CHD8-bound promoters in neurons. **c**, In contrast, in promoters of CHD8-unbound genes, no ETS motif was found. The top 30 enriched motifs are shown.

Extended Data Figure 7 | Relevance of CHD8 binding for transcriptional regulation, chromatin remodeling activity, and ASD gene regulation. a, Significance, and odds ratio of CHD8 binding on DEG promoters, which shows stronger binding on downregulated genes in both heterozygous and homozygous CHD8 KO neurons. **b**, CHD8 binding signal is normalized across the genome and plotted in bins of 100 bp upstream and downstream of ELK1. Only the two regions of 500 bp upstream and 500 bp downstream of TSS compared. Significance is calculated Wilcoxon signed-rank test with continuity correction. **c**, University of California Santa Cruz (UCSC) genome browser tracks of CHD8 ChIP-seq signal at ELK1 motif sites, upstream of Neurofibromin 1 (NF1) gene. **d**, Result from Gene Set Enrichment Analysis of shows disease and pathways associated with DEGs in *CHD8*-KO neurons (7). **e**, Plot shows a group of representative chromatin regulating factors with CHD8 peak at the promoter and significant change in gene expression; many downregulated in *CHD8*-KO neurons. **f**, Table for Gene Ontology (GO) and KEGG pathway from DEGs of RNA-seq experiments (homozygous CHD8-KO compare to control neurons). **g**, Table for Gene Ontology (GO) and KEGG pathway enrichment for a gene with ATAC-seq peak change in CHD8-KO experiment (all genes with gain or lost accessibility in KO combined for ontology analysis).

Extended Data Figure 8 | CHD8 promotes chromatin accessibility and transcriptional activation in human neurons. a, Principal component analysis (PCA) for ATAC-seq signal from WT (ΔCre) and homozygous KO (Cre) neurons shows the accurate separation of samples based on the genotype in PC1. Two embryonic stem cell lines (CR1 and CR2) and two technical replicates for each line are used in the experiment. **b**, Heatmap of normalized ATAC-seq signal in cKO homozygous and control neurons from a targeted ES cell line (CR1) and a targeted iPS cell line (CR3) in two technical replicates from each line. **c**, Open or close chromatin in ATAC-seq generally is associated with unregulated and downregulated genes, respectively, which indicates ATAC-seq and gene expression change is generally at the same direction. **d,** CHD8 binding is stronger on sites of chromatin that are loosing the accessibility in ATAC-seq experiment. **e,** Volcano plot depicting each ATAC-seq peak as

one dot. The color indicates the distance of ATAC-seq peak summit from the closest CHD8 peak summit, and the size of the dot reflects CHD8 ChIP-seq peak score. Genomic sites with less ATAC-seq signals in KO cells tend to localize at the immediate vicinity of CHD8 peak. **f,** Representative browser track of ATAC-seq peak and nucleosome occupancy signal on ATF7 gene. This region lost accessibility at KO cells.

Extended Data Figure 9 | CHD8 positively regulates a group of high confident ASD genes in neurons.
a, Boxplots represent log2 scaled fold change of genes that overlap with SFARI list (ASD genes). **b**, CHD8 binds to promoters of 65 ASD genes with the biallelic recessive mutation (overlap is taken from the genes that are not included in SFARI-2020 list). CHD8 target genes in neurons overlap with its target gene list from Cotney *et al*.,2015, in neural progenitor cells (8).

Extended Data Figure 10 | Chromatin state and target genes of CHD8 in ATAC-seq. a, Heatmap represents an enrichment of promoter-associated state at annotated TSS regions. **b,** correlation of CHD8 binding signal with ATAC-seq signal at differential accessible sites in *CHD8*-KO. The color bar is a log scaled fold change of gene expression. **c,** DEGs ranked according to ATAC-seq fold change in promoter accessibility. The number of genes that lost chromatin accessibility in promoters of KO neurons is higher than genes that gain accessibility at promoters.

Extended Data Figure 11 | CHD8 binding to ETS-enriched promoters, functionally depends on ELK1. a, Table of genomic sites selected for ChIP-qPCR assessment; Shown are motifs present, the number of motifs present, peak score, and motif location relative to TSS. We chose peaks with different occurrences of ETS motif to observe possible dependency on motif number, and we also chose a peak with an unrelated YY1 motif (peak 1003=MMADHC gene). **b,** Validation of CHD8 binding on ChIP-seq peaks in CHD8 knockout neurons using ChIP qPCR assay. Strong or weak peaks lose CHD8 binding signals in KO neurons regardless of the type of the motif present on the peak. **c,** Knockdown of ELK1 and ELF4 with short hairpin (shRNA) shows a decrease in total mRNA (bar graph) and a significant reduction of ELK1 protein (western blot).
d, Knockdown of ELF4 does not affect CHD8 binding on either of ETS or YY1 motif sites, suggesting ELF4 does not influence chromatin binding of CHD8. **e**, Average expression of ETS factors shows ELK1 is the only highly expressed ETS gene in differentiated human neurons (average FPKM values taken from wild type neurons).

BIBILOGRAPHY

1. SPARK: A US Cohort of 50,000 Families to Accelerate Autism Research. Neuron. 2018;97(3):488-93. Epub 2018/02/09. doi: 10.1016/j.neuron.2018.01.015. PubMed PMID: 29420931; PubMed Central PMCID: PMCPmc7444276.
2. Yu G, Wang LG, Yan GR, He QY. DOSE: an R/Bioconductor package for disease ontology semantic and enrichment analysis. Bioinformatics (Oxford, England). 2015;31(4):608-9. Epub 2015/02/14. doi: 10.1093/bioinformatics/btu684. PubMed PMID: 25677125.
3. Heinz S, Benner C, Spann N, Bertolino E, Lin YC, Laslo P, Cheng JX, Murre C, Singh H, Glass CK. Simple combinations of lineage-determining transcription factors prime cis-regulatory elements required for macrophage and B cell identities. Mol Cell. 2010;38(4):576-89. Epub 2010/06/02. doi: 10.1016/j.molcel.2010.05.004. PubMed PMID: 20513432; PubMed Central PMCID: PMCPmc2898526.
4. Bailey TL, Boden M, Buske FA, Frith M, Grant CE, Clementi L, Ren J, Li WW, Noble WS. MEME SUITE: tools for motif discovery and searching. Nucleic acids research. 2009;37(Web Server issue):W202-8. Epub 2009/05/22. doi: 10.1093/nar/gkp335. PubMed PMID: 19458158; PubMed Central PMCID: PMCPmc2703892.
5. Davis CA, Hitz BC, Sloan CA, Chan ET, Davidson JM, Gabdank I, Hilton JA, Jain K, Baymuradov UK, Narayanan AK, Onate KC, Graham K, Miyasato SR, Dreszer TR, Strattan JS, Jolanki O, Tanaka FY, Cherry JM. The Encyclopedia of DNA elements (ENCODE): data portal update. Nucleic acids research. 2018;46(D1):D794-d801. Epub 2017/11/11. doi: 10.1093/nar/gkx1081. PubMed PMID: 29126249; PubMed Central PMCID: PMCPmc5753278.
6. Sugathan A, Biagioli M, Golzio C, Erdin S, Blumenthal I, Manavalan P, Ragavendran A, Brand H, Lucente D, Miles J, Sheridan SD, Stortchevoi A, Kellis M, Haggarty SJ, Katsanis N, Gusella JF, Talkowski ME. CHD8 regulates neurodevelopmental pathways associated with autism spectrum disorder in neural progenitors. Proceedings of the National Academy of Sciences of the United States of America. 2014;111(42):E4468-77. Epub 2014/10/09. doi: 10.1073/pnas.1405266111. PubMed PMID: 25294932; PubMed Central PMCID: PMCPmc4210312.
7. Subramanian A, Tamayo P, Mootha VK, Mukherjee S, Ebert BL, Gillette MA, Paulovich A, Pomeroy SL, Golub TR, Lander ES, Mesirov JP. Gene set enrichment analysis: a knowledge-based approach for interpreting genome-wide expression profiles. Proceedings of the National Academy of Sciences of the United States of America. 2005;102(43):15545-50. Epub 2005/10/04. doi: 10.1073/pnas.0506580102. PubMed PMID: 16199517; PubMed Central PMCID: PMCPmc1239896.
8. Cotney J, Muhle RA, Sanders SJ, Liu L, Willsey AJ, Niu W, Liu W, Klei L, Lei J, Yin J, Reilly SK, Tebbenkamp AT, Bichsel C, Pletikos M, Sestan N, Roeder K, State MW, Devlin B, Noonan JP. The autism-associated chromatin modifier CHD8 regulates other autism risk genes during human neurodevelopment. Nature communications. 2015;6:6404. Epub 2015/03/11. doi: 10.1038/ncomms7404. PubMed PMID: 25752243; PubMed Central PMCID: PMCPmc4355952.